

Nano-onion necklaces and graphene flake
decorated polyaniline: biodegradable
nanowires for neuroregenerative
medicine

Final Report

Joseph Smith

Supervisor: Richard Jackman

Second Assessor: Neil Curson

March 2013

Abstract

In designing a biodegradable conduit for nerve regrowth surgeons have a material that lacks a crucial property. Neurons are essentially analogue to digital converters: electronic components that require a good electrically conductive growth medium. This project proposes to provide this cost-effectively by wiring in novel biodegradable nanowires. Two unique nanowire candidates are designed, synthesised, and evaluated.

Initially, the report looks at a nano-necklace. SEM images show excellent wire construction when linking carbon nano onions with a biodegradable cyclodextrin-oxydianiline complex. FTIR analysis evidence the complex forming. However, EIS shows the available nano onions insulates and this serves only as a structural viability study.

As an alternative nanowire we look to improve the conductivity of polyaniline, an electroactive polymer, by nanocompositing with graphene. At a mass ratio of 1 part graphene to 100, our synthesised material fits a variable range hopping mechanism well and displays a $\sim 10 \text{ S cm}^{-1}$ conductivity. At a 1:1 ratio, the material behaves metallicity. It has a heightened conductivity of around 100 S cm^{-1} and a resistivity which increases with temperature. SEM shows this material is partially fibrous and future work is detailed to improve this structure.

Improving neuroregeneration by use of a conduit interfaced with nanowires proposed here will have a profound impact as peripheral nerve trauma accounts for 3% of all injuries. The embedded nanowire, if successful, may provide a standard for future bioengineered devices.

Contents

Contents	ii
List of Figures	iv
Nomenclature	vii
1 Introduction	1
2 Background: Use of a biodegradable nanowire in a nerve conduit	2
3 Experimental Methods	6
3.1 Electrochemical Impedance Spectroscopy	6
3.2 Fourier Transform Infrared Spectroscopy	7
3.3 Atomic Force Microscopy	8
3.4 Scanning Electron Microscopy	8
4 The Nano Onion Necklace	9
4.1 The Carbon Nano Onion: Physical and Electronic Characterisation	9
4.1.1 Overview	9
4.1.2 Experimental Procedure	9
4.1.3 Results	10
4.1.4 Discussion	13
4.2 Preparing the Inclusion Complex	16
4.2.1 Overview	16
4.2.2 Experimental Procedure	17
4.2.3 Results	18

4.2.4	Discussion	18
4.3	Beading the nano-onion necklaces	21
4.3.1	Overview	21
4.3.2	Experimental Procedure	22
4.3.3	Results	22
4.3.4	Discussion	24
5	Graphene decorated Polyaniline	28
5.1	Initial Interfacial Polymerisation of Aniline	28
5.1.1	Overview	28
5.1.2	Experimental Procedure	29
5.1.3	Results	30
5.1.4	Discussion	30
5.2	Graphene Oxide and Polyaniline	31
5.2.1	Overview	31
5.2.2	Experimental Procedure	32
5.2.3	Results	32
5.2.4	Discussion	33
5.3	Modifications and Further Analysis	39
5.3.1	Overview	39
5.3.2	Results	39
5.3.3	Discussion	40
5.4	Polyaniline Nanofibres	47
5.4.1	Overview	47
5.4.2	Experimental Procedures	47
5.4.3	Results	47
5.4.4	Discussion	47
6	Conclusions	49
	References	51

List of Figures

2.1	The neuron, taken from [1]	3
2.2	Schwann cells forming Bands of Bungner to repair a damaged peripheral nerve, adapted from [2]	4
2.3	Diagrammatic representation showing the benefits of high-aspect fillers in percolation systems	4
2.4	Schwann cells grown on UCL-NanoBio, from [3]	5
2.5	Left: A C ₆₀ molecule, adapted from [4]. Right: A nano onion cross section as seen in [5]	5
4.1	Impedance response of Carbon Nano Onions at different temperatures	11
4.2	Circular fit to Cole-Cole plot of CNOs at Room Temp under deeper vacuum	11
4.3	FTIR spectra of nano onion sample	12
4.4	The test microstructure	13
4.5	Nano onions imaged at 8 μ m	14
4.6	Smaller AFM resolutions show loss of clarity	15
4.7	The reflux setup	19
4.8	The formed inclusion complex	19
4.9	Buchner flask and funnel setup	20
4.10	Vacuum drying the inclusion complex	20
4.11	FTIR of the reactants and product from the inclusion complex synthesis	21
4.12	Sonicated nano onions	23
4.13	The inclusion complex dissolved in DMF	23

LIST OF FIGURES

4.14	Layers of the composite product	24
4.15	SEM images of the unwashed sample.	25
4.16	SEM images of the washed sample	26
5.1	The interfacial polymerisation reaction system	30
5.2	Attachment between graphene oxide and polyaniline from [6]	31
5.3	The oxidation solution	33
5.4	After the addition of H_2O_2	34
5.5	Graphite oxide	34
5.6	Suspension of graphene oxide in aniline	35
5.7	pAni-GO composite stirred under ice bath	35
5.8	The filtered pAni-GO composite	36
5.9	SEM on the pAni-GO	37
5.10	Electrochemical Impedance Spectroscopy on the pAni-GO	38
5.11	AFM of graphene oxide	40
5.12	The surface was uneven and porous in places	40
5.13	SEM on the second pAni-GO synthesis	41
5.14	EIS on the second synthesis	42
5.15	The second synthesis shows a much higher resistivity than before	43
5.16	Resistance plotted against temperature shows distinct trends for the two ratios	43
5.17	1:100 PANi-GO with Mott Variable Hopping Fit	44
5.18	1:1 PANi-GO with quadratic temperature fit	44
5.19	SEM on pAni	48

Nomenclature

Roman Symbols

C_n capacitor n

f frequency in Hertz

G conductance in Siemens

R_n resistor n

T temperature

Z impedance in Ohms

Greek Symbols

Ω Ohms

μ $\times 10^{-6}$

ω angular frequency in rads^{-1}

π $\simeq 3.14\dots$

ρ resistivity

σ conductivity

Superscripts

' real component

" imaginary component

Other Symbols

exp the exponential function

$\Im\{\}$ imaginary component

ln the natural logarithm

$\Re\{\}$ real component

Acronyms and Abbreviations

3D 3 dimensional space

AFM Atomic Force Microscopy

ATR Attenuated Total Reflection

CNO Carbon Nano onion

DLS dynamic light scattering

DMF dimethylformamide

EIS Electrochemical Impedance Spectroscopy

FTIR Fourier Transform Infrared Spectroscopy

GO graphene oxide

IPO Isopropanol

ND nanodiamond

NMR nuclear magnetic resonance

PAni polyaniline

RCF relative centrifugal force

RPM revolutions per minute

SEM Scanning Electron Microscopy

Chapter 1

Introduction

This project has been undertaken to research feasible nanowire candidates for deployment in biological surroundings. These wires have been designed to provide strong electrical conductivity in a new tubular device for neuronal repair, termed a *conduit*, before biodegrading and leaving the body safely once repair is complete.

In Chapter 2, the biology of the neuron is reviewed, problems with current medical techniques shown, and the need for this alternative strategy proven. The value of seeking a biodegradable nanowire will be evidenced by discussing conductivity through percolation and the advantage of adopting a high-aspect filler. In Chapter 3, the purpose of key analytical techniques used in this project is given. Basic principles are used to explain the operation of each with clarity.

In Chapter 4, the first work chapter, synthesis and characterisation of a nano-necklace is presented. First, the nano onion is characterised using FTIR, AFM and EIS. The necklace is synthesised and characterised using FTIR before the nanoparticles are added and SEM performed.

In Chapter 5, work progresses to the study of an alternative strategy looking at graphene nanoparticles on a polyaniline backbone. Several variants of this composite are synthesised and electrically analysed using EIS, with bulk conductivity calculations and temperature dependences explored, before physically characterising through SEM.

Chapter 6 concludes this report by summarising this work and detailing future research to take these novel candidates towards refinement, production, and use in the intended medical application.

Chapter 2

Background: Use of a biodegradable nanowire in a nerve conduit

A *neuron* is a cell that transmits electrical signals. It can be thought of as an analogue to digital converter. The cell takes in multiple inputs from branched connections or *dendrites* attached to it and sends a pulse response along its long tail or *axon* (see Fig 2.1). Neurons form a network through the body termed the peripheral nervous system, distinguished from the central nervous system of the brain and spine. Damage to the peripheral nervous system, caused when the tissue is crushed, stretched, or lacerated due to sharp objects [7], accounts for 3% of all trauma injuries [8].

After trauma occurs, the nerve attempts reparation. First, the stump of the axon furthest from the injury degenerates [9]. The near stump sends axonal sprouts. Schwann cells are generated and align to form columns, termed *Bands of Bungner*, which direct axonal regeneration towards the target nerve end as shown in Fig 2.2 [10, 11].

Injuries beyond the regenerative capabilities of the tissue must be surgically operated on. The established technique is to harvest donor nerve tissue from another part of the body to bridge between two nerve ends [3, 7, 12, 13]. Several difficulties can occur here. Donor tissue may be the wrong diameter or of insuffi-

cient length. Surgery from harvesting tissue introduces disease termed *donor site morbidity* [3, 7, 12] resulting in permanent loss of feeling in almost all cases [14].

Using a synthetic *conduit* is a viable alternative. A conduit approximates nerve stumps by constraining regeneration along its cylindrical shape. Bioengineers design conduits that are as architecturally similar to the injured nerve as possible [7]. The base polymer for the conduit to has been developed at UCL and is trademarked *UCL-NanoBio* [15]. It retains mechanical strength in biological surroundings [16] yet is biodegradable hence removal surgery to prevent scar tissue forming, compressing the nerve, is not required [2].

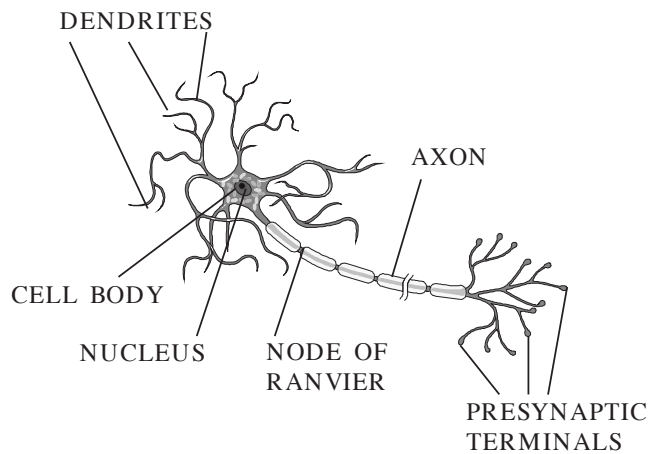


Figure 2.1: The neuron, taken from [1]

As neurons are biological electronic components, optimal regeneration occurs in an electronically conductive environment. This has been verified experimentally by Zhang [17]. Adding small quantities of conducting nanoparticles to UCL-NanoBio should vastly improve conductivity through *percolation* [18]. Each location in the polymer now has a probability of being occupied by a conducting particle. At low concentration, conducting sites are isolated or form small clusters. A cluster exists in which two or more nano onions are linked by a conducting path. As concentration is increased, these conducting paths grow. At some threshold, current will be able to *percolate* from one edge of the polymer to the other. The probability of conduction is near binary about this threshold value [19].

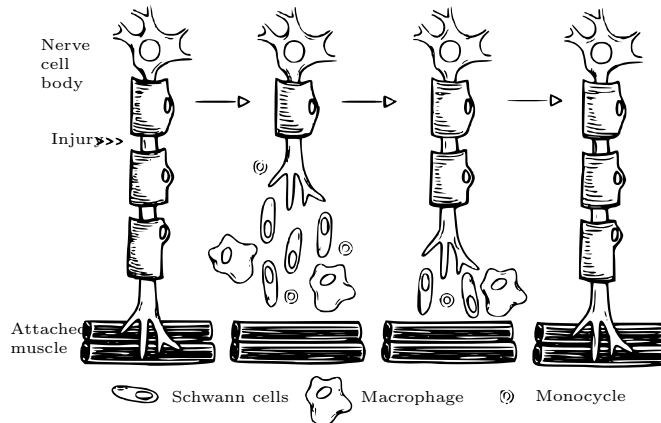


Figure 2.2: Schwann cells forming Bands of Bungner to repair a damaged peripheral nerve, adapted from [2]

The aspect ratio of the conducting molecule is a central factor to determine percolation threshold [20, 21]. Research shows far smaller amounts of materials like carbon nanotube or silver nano-wires, with large length to diameter ratios, are required to achieve threshold [22, 23]. A diagrammatic explanation is shown in Fig 2.3. On the left, 84 particles with 1:1 aspect ratio have their centres randomised. There is a low probability that a conduction path will stretch from one side to the other. In contrast, with the 84 high aspect particles, there is often many conduction paths from one side of the material to the other. Reducing the amount of nanoparticles needed for suitable conduction would make the conduit significantly cheaper. A way to achieve this is to include high aspect ratio fillers.

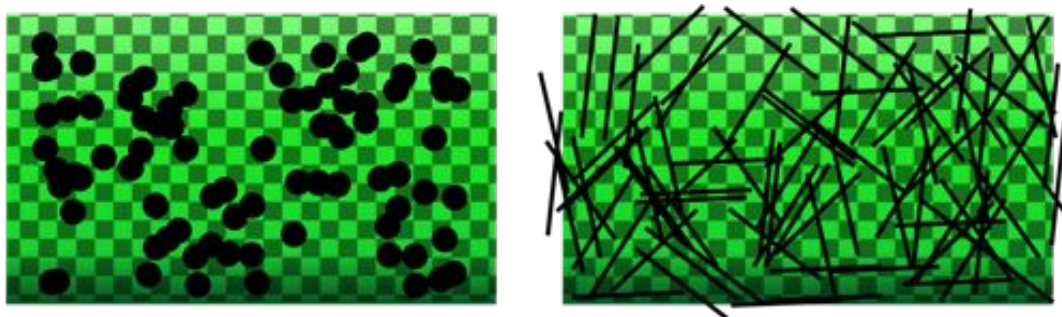


Figure 2.3: Diagrammatic representation showing the benefits of high-aspect fillers in percolation systems

However, an essential purpose of the conduit is that it biodegrades after tissue

repair. Any high aspect ratio filler must also be capable of biodegradability. Nanoparticles below 6nm are processable by leaving the bloodstream through the kidneys [24]. This project aims to produce a suitable synthesis to link conducting particles by some biodegradable form.

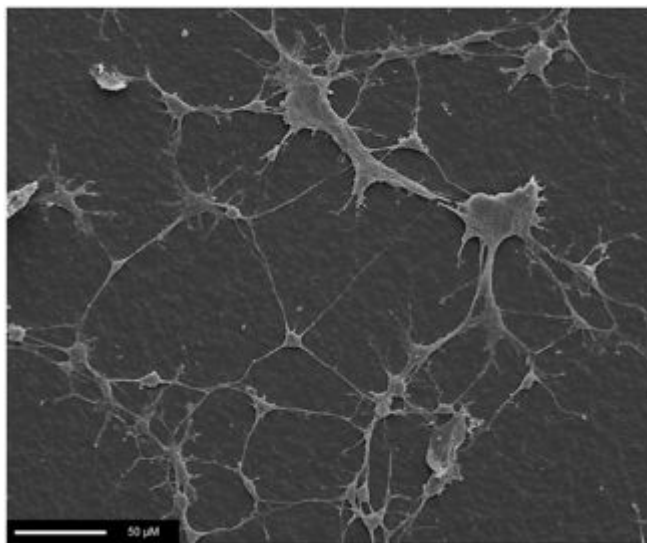


Figure 2.4: Schwann cells grown on UCL-NanoBio, from [3]

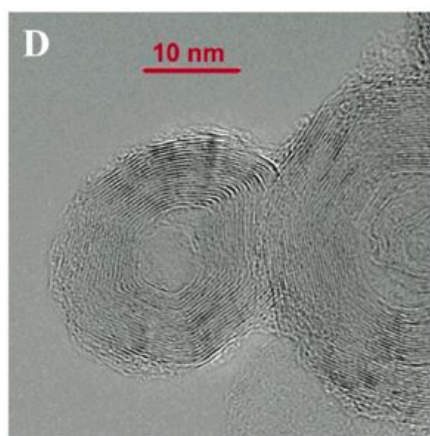
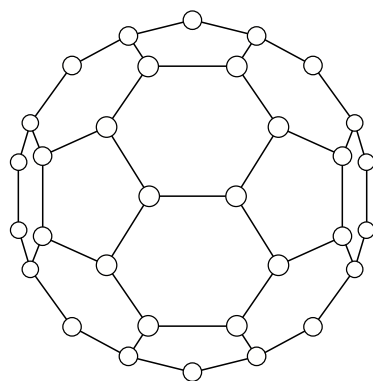


Figure 2.5: Left: A C_{60} molecule, adapted from [4]. Right: A nano onion cross section as seen in [5]

Chapter 3

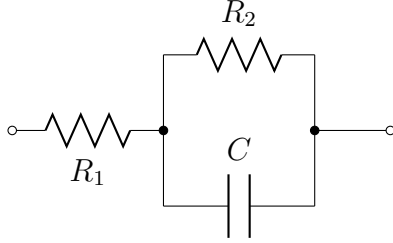
Experimental Methods

As devices are designed and produced, they must be evaluated for their structural and electronic capabilities. This will be achieved using a combination of imaging and spectroscopic techniques. In this chapter, the benefit offered by each characterisation procedure will be evidenced and explained using simple principles.

3.1 Electrochemical Impedance Spectroscopy

Electrochemical Impedance Spectroscopy (EIS) measures the impedance at a range of frequencies. A sinusoidal voltage is applied and the current through the sample is measured. By observing the phase shift between input and output signals, the capacitance can be measured. By observing the amplitude shift, a value for the material conductivity can be found. Two electrically conducting electrodes are placed touching the sample surface. The sample is electrically shielded by a stainless steel chamber which can be pumped down to perform measurements in vacuo.

The most important result is the Cole-Cole plot which plots the imaginary impedance (denoted as Z'') against the real component (denoted as Z'). Each point corresponds to a different frequency. From this, a circle can be fitted to determine the resistance of the sample. The impedance of an electrochemical cell like the nano onion is modelled as a resistor in series with a single time constant [25].



$$Z(\omega) = R_1 + \frac{R_2(1 - j\omega R_2 C)}{1 + (\omega R_2 C)^2} \quad (3.1)$$

$$\Re\{Z\} = R_1 + \frac{R_2}{1 + (\omega R_2 C)^2} \quad (3.2)$$

$$\Im\{Z\} = \frac{-\omega R_2^2 C}{1 + (\omega R_2 C)^2} \quad (3.3)$$

Substituting for Omega

$$(\Re\{Z\} - R_1 + R_2/2)^2 + \Im\{Z\} = (R_2/2)^2 \quad (3.4)$$

This is analogous to a circle with a radius $R_2/2$ and a centre at $(R_1 + R_2/2, 0)$. Hence fitting a circle allows this value to be found. The capacitance is determined by finding the cut-off frequency and using

$$f_{3\text{dB}} = \frac{1}{2\pi R_2 C} \quad (3.5)$$

Characterising the capacitance and, most importantly, the conductive merits of materials will assess their suitability in providing electrical conduction.

3.2 Fourier Transform Infrared Spectroscopy

A Michelson interferometer uses a moving mirror to send a range of infrared wavelengths at a chemical bond simultaneously. The molecule absorbs the signal and oscillates at a frequency that generates an electric dipole and interferes with the incident beam. Both the bond strength and the mass of the atoms set the frequency like the spring constant and particle mass in simple harmonic motion. A Fourier transform enables all reflected wavelengths to be analysed and

a spectrum produced to show which are absorbed. By observing a peak at a certain frequency, the functional group that would produce this can be identified, allowing the characteristic fingerprint of a molecule to be evidenced. Using this technique provides confirmation that the expected chemistry has taken place and that a material is as theory suggests whilst highlighting unexpected functional groups.

3.3 Atomic Force Microscopy

A probe on the end of cantilever interacts with the sample surface. Van der Waals forces between the probe and sample causes the cantilever to move. The cantilever arm reflects a laser beam onto a position aware photodetector. As the cantilever moves, the photodetector records the position of the laser focus point. With nanoparticles, the AFM operates in tapping mode. The cantilever oscillates near resonant frequency over the sample surface. The surface interactions causes the oscillation amplitude to vary the damping is measured. The AFM should build up a 3D representation of the surface from this data. A vacuum is not required so the material can be imaged in its natural environment. Using AFM should allow surface features of a sample to be imaged in 3D providing evidence of its structure.

3.4 Scanning Electron Microscopy

An SEM images a sample by scanning with a beam of electrons. A cathode creates a high energy thermionic electron beam that is repelled by electrons at the surface of the sample. Some elastically scatter and form a primary electron current. Alternatively, some surface electrons are repelled enough that they are emitted from the atom and attracted to the positively charged detector. This is the secondary electron current which is recorded against the position of the probe on the surface to produce a topographical image. This will give key insight into the morphological make up of a sample and will be vital, for instance, in determining whether a composite provides the fibrous wire structure intended.

Chapter 4

The nano-onion Necklace

4.1 The Carbon nano-onion: Physical and Electronic Characterisation

4.1.1 Overview

Concentric rings of graphene encasing a C_{60} molecule (see Fig 2.5), termed the nano-onion, can be made from ND [26] and other notable methods [27, 28]. Nano-onions are nontoxic in a cellular environment [29] and crucially, their sub 5nm size makes them processable [24]. They have been found to have a conductivity of up to $4S\text{cm}^{-1}$ under certain growth techniques [30].

The first experimental work performed is to physically and electronically characterise the carbon nano-onion. It is essential to observe the onions are strong electrical conductors suitable for use in the nanowire and of the nanoscale size suggested in the literature. Identifying the function groups on the surface of the nano-onion using FTIR gives more precise information about the specific nano-onion species. Treatment with specific functional groups may provide optimal conductances [31].

4.1.2 Experimental Procedure

EIS was carried out using the Solartron impedance analyzer SI1260A. A sample of nano-onions in a crucible was placed in the chamber. The needles were positioned

carefully to ensure contact was made with the surface yet did not short-circuit. The sample was put under vacuum to around 10^{-2} mBar. The vacuum pump vents from below, preventing the powder from being disturbed.

In FTIR, Attenuated Total Reflection (ATR) mode is used for solid materials like the nano-onion. The module on top of the machine measures the intensity of the reflected beam as opposed to transmitting light through the material. The surface is cleaned with isopropanol (IPO). Nitrogen purging is used to cleanse the chamber of contaminant chemicals. A background sample is taken which is subtracted from the image to remove the presence of trace contaminants. A tweezer full of carbon nano-onions is added to several millilitres of acetone. A pipette is used to drop the mixture onto the ATR interface.

Two SiO_2 squares were added to a solution of CNOs in DMF (dimethylformamide). Ten hour sonication embedded the onions into the silica surface, operating at 100% amplitude. The water level of the sonicator was topped up to cover the sample vessels. One sample was washed with water in an attempt to obtain a monolayer of the onions on the silica surface. The samples were dried overnight and a test microstructure was imaged to calibrate the AFM. Both samples were imaged in non-contact mode using a variety of resolutions.

4.1.3 Results

4.1.3.1 Electrochemical Impedance Spectroscopy

The onions were heated from room temperature to 200°C in 50°C increments and the impedance recorded. Higher temperatures would permanently degrade material properties. Fig 4.1 shows the impedance response. At all temperatures, the carbon nano-onions have a low pass characteristic. Overnight, the chamber was pumped down to a deeper vacuum of $5.65\mu\text{Bar}$ and measurements retaken, shown in red on the plot. Further removal of contaminant particles provides higher accuracy. Using the analytical techniques described in the previous chapter, the figure can be fitted with a very large calculated resistance of $5.39 \times 10^{12}\Omega$ to the deep vacuum data.

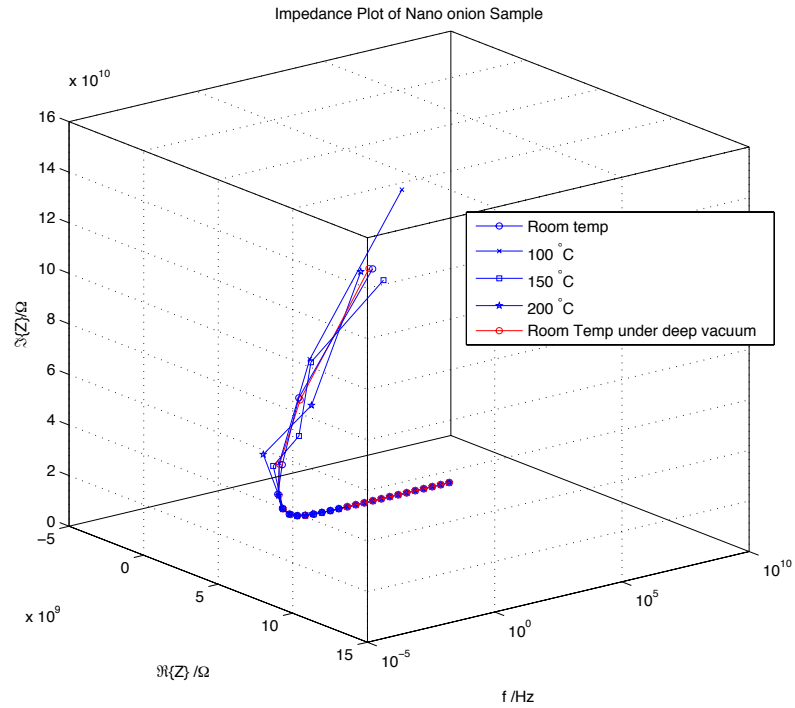


Figure 4.1: Impedance response of Carbon nano-onions at different temperatures

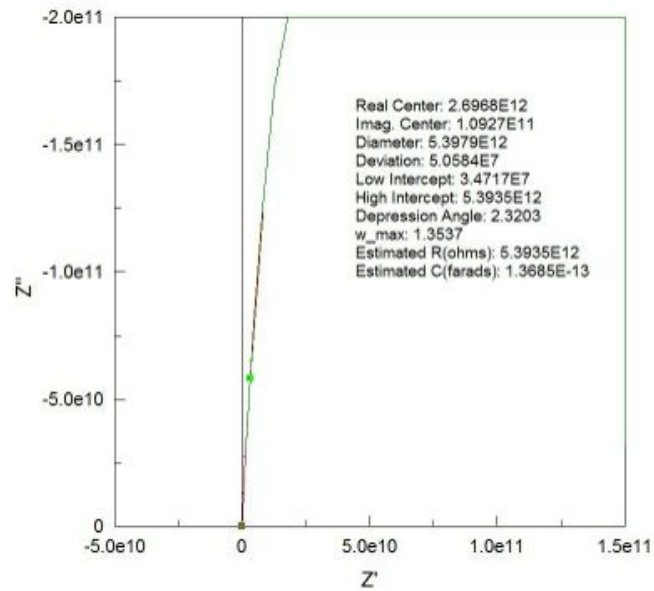


Figure 4.2: Circular fit to Cole-Cole plot of CNOs at Room Temp under deeper vacuum

4.1.3.2 FTIR Analysis

In the onion, carbon-carbon bonds are symmetric so only the surface terminations will be observed. Symmetrical bonds do not have the dipoles discussed in the FTIR spectra. Two plots are shown in Fig 4.3. The initial shows clear baseline shifting. The following day, a good spectrum was observed with peaks in similar places without the shift. The dominant peaks are at 2900cm^{-1} , 1750cm^{-1} , 1250cm^{-1} and 1050cm^{-1} .

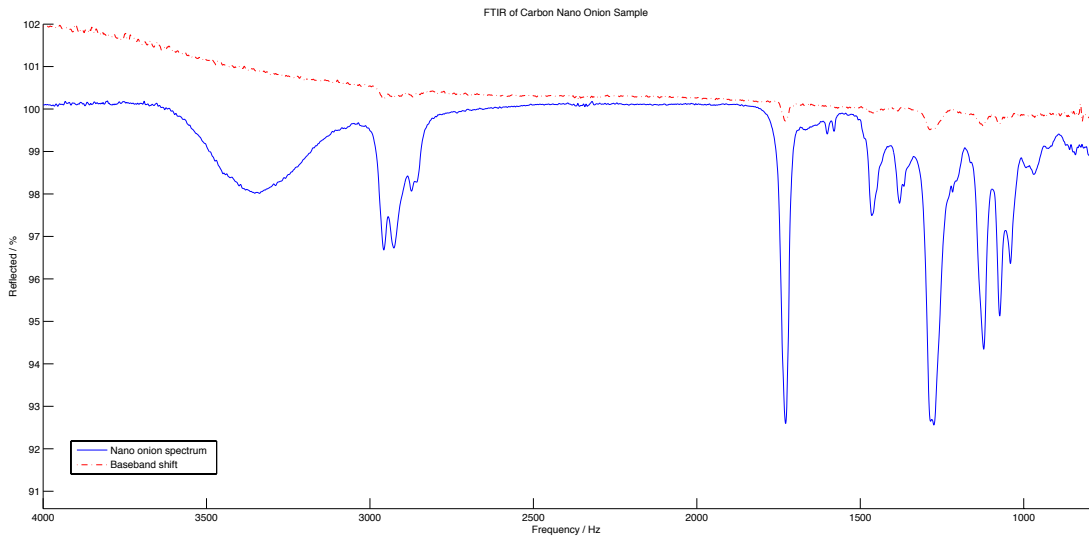


Figure 4.3: FTIR spectra of nano-onion sample

4.1.3.3 AFM

A clear image of the microstructure is seen in the test image in Fig 4.4. From the topography image, black rectangles are evenly spaced with a feature size of $10\mu\text{m}$ by $10\mu\text{m}$. These are dents in the surface corresponding to around $0.1\mu\text{m}$ as shown on the bottom graph of this figure.

The sample has been imaged at $8\mu\text{m}$ successfully in Fig 4.5 but the features needed are at several orders of magnitude lower than this. Sharp $0.1\mu\text{m}$ by $2\mu\text{m}$ scratches in the sample are seen. Imaging at higher resolutions to look for nanoscale features is less successful. In Fig 4.6, a strong horizontal noise component in the data is seen. As resolution increases, noise obscures the underlying

image further. The intention to see the size of these particulates has not been achieved.

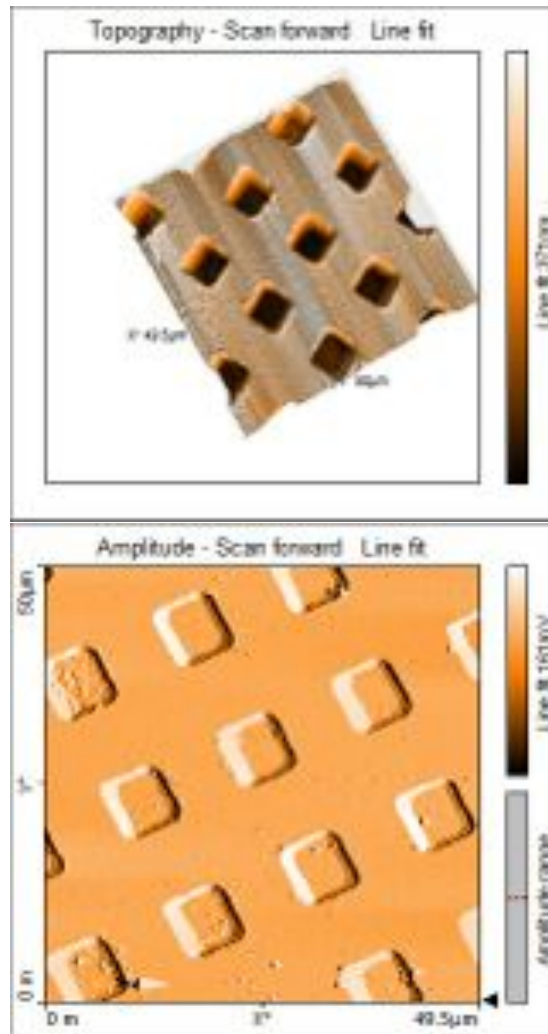


Figure 4.4: The test microstructure

4.1.4 Discussion

4.1.4.1 Electrochemical Impedance Spectroscopy

EIS analysis in Fig 4.1 indicates this nano-onion sample has an extremely high resistance. At $5.39 \times 10^{12}\Omega$, the particles cannot be used to build conducting nanowires. Modifying the surface terminations of the material with nitrogen,

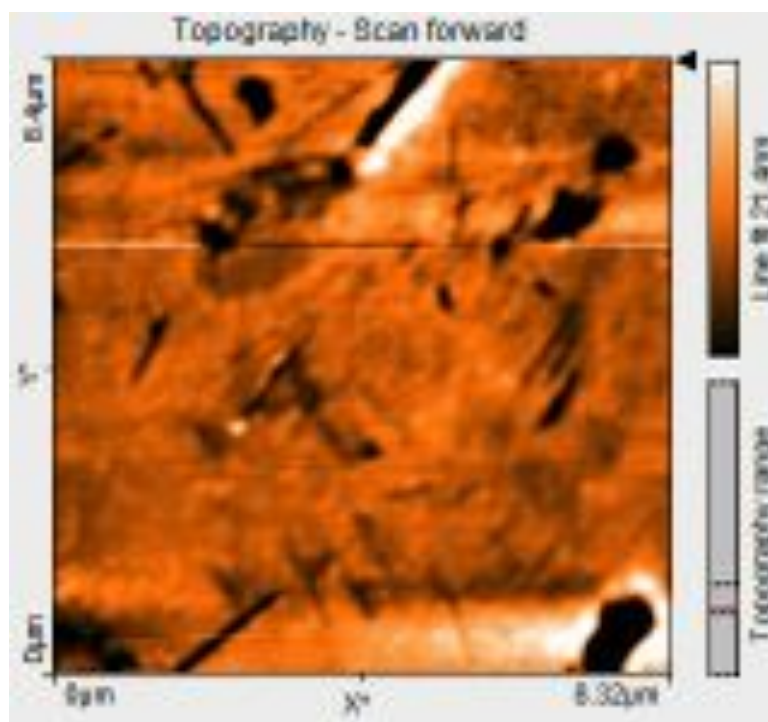


Figure 4.5: nano-onions imaged at $8\mu\text{m}$

hydrogen, or ozone may improve conducting properties [31]. The next task will be to characterise the sample with FTIR to see current surface terminations.

4.1.4.2 FTIR Analysis

There was no nitrogen available so some contaminants may be present in the spectrum. The base line shifting in Fig 4.3 is due to refraction by macromolecular clusters and is a known phenomenon in carbon samples [32]. By subtracting the gradient in the void region between $2500\text{-}2000\text{cm}^{-1}$, occupied solely by heavy atoms and triple bonds, this could be eliminated. Characteristic peaks are apparent that can be identified using a lookup table [33]. A peak at 2900cm^{-1} is characteristic of a C-H bond. One peak at 1750cm^{-1} is characteristic of carbonyl groups (C=O). A strong peak at 1250cm^{-1} is an ester vibration. This may be due to not all traces of acetone being eliminated in the background scan. There is another peak at 1050cm^{-1} which is also characteristic of a C-O bond.

Luszczyn et al [29] FTIR oxidised CNO in ATR mode. The analysis focuses

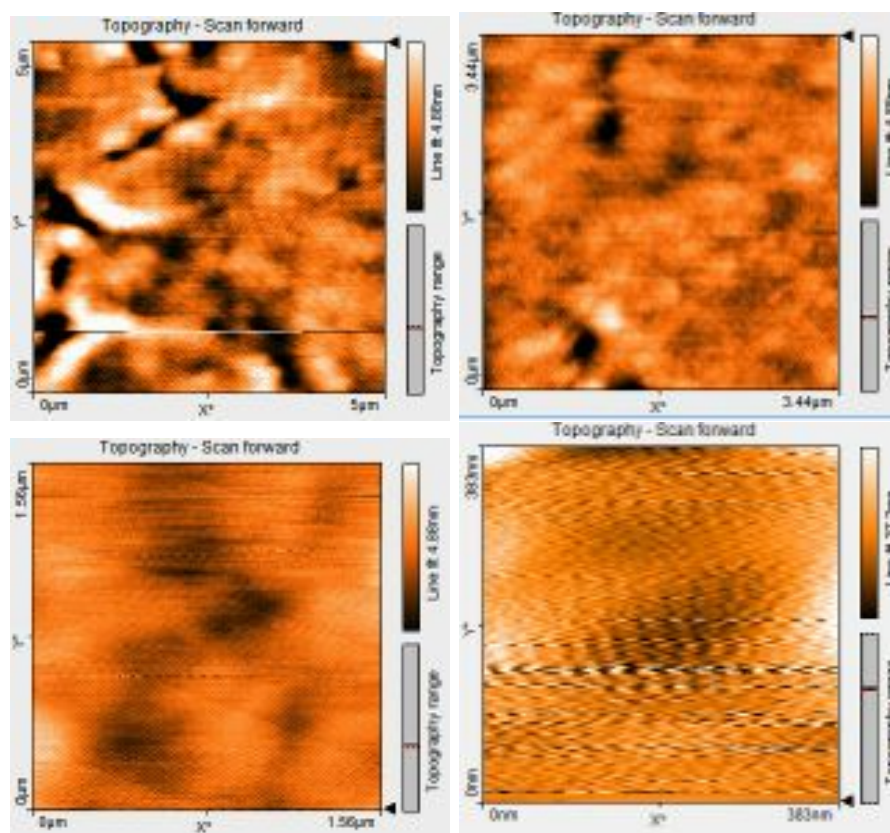


Figure 4.6: Smaller AFM resolutions show loss of clarity

on the 1500-1750 band in which they similarly identify prominent peaks for C=O stretching at 1743, 1734 and 1714 cm^{-1} . Zhou et al [34] underwent FTIR on hydroxy-CNOs and similarly note sp^3 C-H stretching at 2926 and 2858 cm^{-1} .

These nano-onions have evident oxygenated surface terminations. A deeper study would look to add different functional groups such as nitrate and ozone and, with EIS, see the affect on conductivity. However, new carbon nano-onion species cannot currently be synthesised in the laboratory; this device based project will focus on material application.

4.1.4.3 AFM

Fig 4.4 shows AFM is a strong technique for imaging microstructures. However, imaging nanostructures was futile as the device picked up noise vibrations, possibly from telecommunications signals. This is seen clearly in Fig 4.6 when increasing the resolution from $5\mu\text{m}$ to $0.3\mu\text{m}$. Luszczyn et al[29] used AFM to monitor the effect of CNO films on other substrates, and this proved more suitable than analysing individual particulates. Zhou et al [34] were able to estimate nano-onion diameters of around 85nm by embedding in polystyrene. They note particles were otherwise too aggregated. However, these onions are over an order of magnitude greater than our sample. The highest resolution $10\mu\text{m}$ Nanosurf scanhead was used for two weeks of imaging. It has not been evidenced that the carbon particulate are nano-onions and may be amorphous. Zhou et al show representative images of CNOs using SEM. In future, this will be adopted with higher resolution expected. New onions cannot currently be produced in the laboratory so the sample will be used regardless of analysis results.

4.2 Preparing the Inclusion Complex

4.2.1 Overview

The next stage is to produce the host polymer for the nano-onion. In the proposed synthesis, each onion is contained within two opposing cyclodextrin units, a cylindrically shaped glucose with a usefully large cavity [35]. A similar structure has been built using C_{60} [36] in which the cyclodextrin acts to solubilise the

fullerene in water whilst retaining its intrinsic properties. Cyclodextrin should attach to the nano-onions by forming an inclusion complex with oxydianiline. When nerve reparation is complete, the inclusion complex will biodegrade letting the nano-onions leave the body via the blood stream as shown by Choi et al[24].

Initially, the cyclodextrin is mixed with the oxydianiline as detailed by Yang [37]. This procedure was chosen personally from the literature survey. Crystal filtration is achieved using a Buchner flask and funnel. The solution is poured onto filter paper on top of the funnel. A vacuum pump is attached and the liquid is drawn through the funnel by suction. The crystals remains on the paper to be collected. Further liquid content is removed by drying the crystals in a vacuum. The dried product can be weighed to obtain the yield. It is expected the yield will be low as this is the first time the procedure has been performed and the experimenter has limited experience. The best way to determine if the product is the expected inclusion complex is to analyse its chemical signature with FTIR as used with the nano-onions. The peaks present in the product can be matched to those in the reactants.

4.2.2 Experimental Procedure

In a round-bottom flask half-full of deionised warm water, 2g (10mmol) of oxydianiline was added to 11.35g (10mmol) of β -cyclodextrin. The material was measured on a pan balance. Shutting the perspex case prevents air currents disturbing measurements. The round-bottom flask was held in an oil bath at 190°C for 6 hours under reflux using a Liebig condenser. The mixture was agitated constantly for the duration using a magnetic stirrer at a medium speed. The condenser, purchased from Sigma Aldrich, was used to prevent product evaporating during stirring. It is water cooled as the mixture is heated.

The solution was cooled over the weekend in a 4°C fridge and crystallised. The solution was vacuum filtered using a Buchner flask and funnel. The collected crystals were scraped from the filter paper and dried in a vacuum chamber overnight. The crystals were weighed using a pan balance. The reactants and product were characterised using FTIR, operating in ATR mode. A force of 30N was applied to each sample to observe strong peaks. Eight scans were carried

out and the average taken to eliminate noise. The surface was cleansed with IPO between samples and new background spectra taken.

4.2.3 Results

Fig 4.7 depicts the reflux setup with the round bottom flask held above an oil bath which is heated at 190°C with the magnetic stirrer. The oil heat was chosen such that small stable bubbles appeared on the water surface. Attached to the round bottom flask is the water cooled Liebig condenser. There was not time to perform a six hour reflux so the system was left overnight. Fig 4.8 shows the crystalline reactants dissolved completely in the water and a yellow solution formed. Fig 4.9 shows the solution filtered over a Buchner flask to collect a uniform red crystal product. The colour of the crystals changed to brown on drying as seen in Fig 4.10. The product was weighed at $0.676\text{g} \pm 0.005$.

Fig 4.11 shows the spectra of the two reactants, β -cyclodextrin and oxydianiline, for comparison with the product. It is observed that the product shares peaks with oxydianiline at 1500cm^{-1} and 1250cm^{-1} . A clear peak shared with cyclodextrin is seen at 1050cm^{-1} . Other less defined spectral areas also match.

4.2.4 Discussion

Yang et al [37] report the same yellow viscous solution forming from a transparent solution when the powders dissolved. Yang et al [37] achieved a 90% yield in producing the inclusion complex. Here, 50 times the $0.676\text{g} \pm 0.005$ product was used as reactants and so the yield is less than 2%. Considerable product was lost in scraping from the Buchner funnel. Additionally, the product was not refrigerated immediately preventing perfect crystallisation. The reflux was left for the weekend as opposed to 6 hours so contaminants may have entered the mixing vessel. However, the yield is high enough for experimental work to continue and the nanowires to be fabricated which is the essential objective.

From Fig 4.11, it is evident the inclusion complex shares peaks from both reactants that can be identified using a lookup table [33]. From this table, those shared with oxydianiline: 1500cm^{-1} may be identified as an arene group and 1250cm^{-1} as an ester link (C-O-C). The cyclodextrin peak at 1050cm^{-1} can be

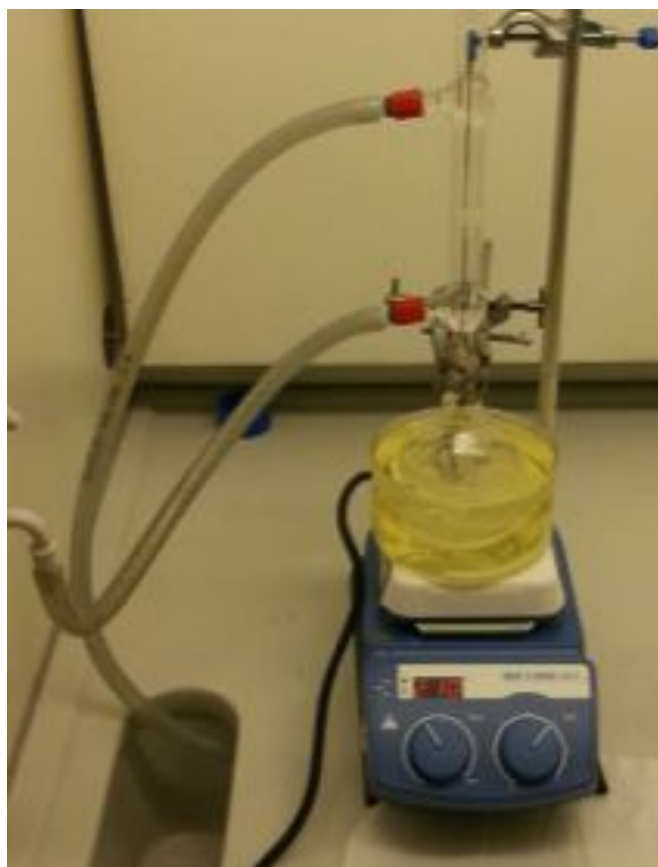


Figure 4.7: The reflux setup



Figure 4.8: The formed inclusion complex



Figure 4.9: Buchner flask and funnel setup



Figure 4.10: Vacuum drying the inclusion complex

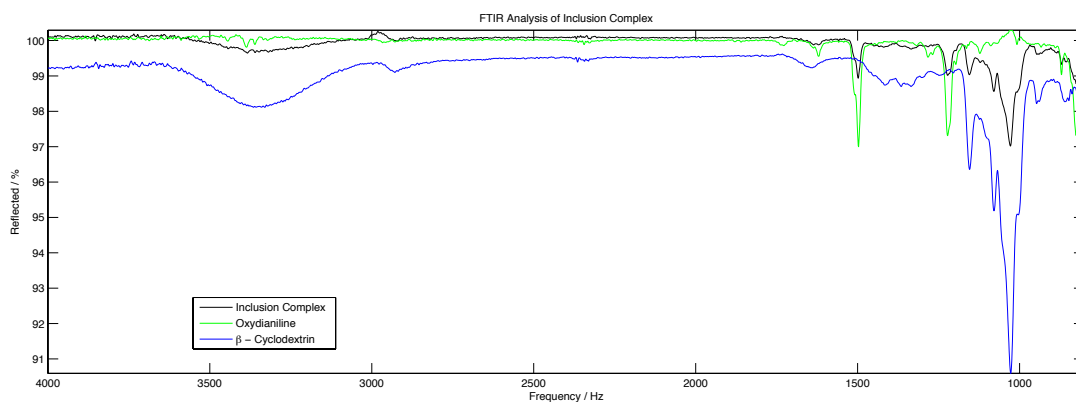


Figure 4.11: FTIR of the reactants and product from the inclusion complex synthesis

identified as a hydroxyl group (C-OH). Yang et al [37] identify the same aromatic C=C bond at 1503cm^{-1} . They identify a peak at 1227cm^{-1} as C-N which could be that identified as C-O-C herein. There is ambiguity identifying peaks even for the skilled chemist. No further FTIR peaks are identified for the paper focuses on NMR spectroscopy. As the spectrum of the product matches peaks from each reactant the inclusion complex has been synthesised correctly. The single crystal form evidences against the consideration that the product is merely a mixture of the reactants.

4.3 Beading the nano-onion necklaces

4.3.1 Overview

For even addition to the inclusion complex, it is necessary to achieve a good dispersion of nano-onions through ultrasound sonication. Centrifugal treatments clean and extract the material. Using an SEM technique should prove more suitable than AFM to produce an image of the composite. A fibrous wire like material will be observed if the synthesis has been successful.

4.3.2 Experimental Procedure

A 14mg sample of nano-onions were sonicated for 52 minutes in 100ml of dimethylchloride at 280kJ (50% horn amplitude). 0.267g (0.02mmol) of the inclusion complex was added to 10ml of DMF until fully dissolved. This was added in 1ml increments to the sonicated sample in 5 minute intervals. The solution settled for 72 hours to form layers. Using a pipette, samples from the three layers were extracted into 1ml centrifuge tubes. The solution was remixed with a magnetic stirrer and samples were extracted from the solution for centrifuging. The centrifuge was set at 1000RPM, equivalent to 8609RCF, and operated for five minutes. A dense pellet of material collected at the bottom of the solution. The top liquid was discarded using a pipette with the tube refilled with water. A vortex mixer was used to remix the solution and the centrifugal treatment repeated.

One sample taken from the bottom layer and one from the cleaned material were pipetted onto conducting pieces of silicon and left to evaporate for 24 hours in covered petri dishes. These pieces were imaged using SEM. The images were post-processed by adjusting contrast and exposure to produce a more defined image. Conducting silicon is used to prevent charging effects where the build up of excess electrons can distort images.

4.3.3 Results

After sonication, the nano-onions show a good dispersion [4.12](#). The inclusion complex is seen to dissolve in DMF [4.13](#) to form an orange solution. Three layers form in the product after settling as seen in [Fig 4.14](#). A sample was taken from the bottom layer. Layers were disturbed and did reform well hence adoption of centrifugal treatment to retrieve further product. A well defined pellet was observed on the initial centrifuge. After washing, a much looser pellet was retained. The remaining material was stored in a centrifuge jar. A metal spatula was used to touch the inner jar surface and fibrous material retrieved. It was noted that the jar had melted and remaining material had plastic contaminants.

In [Fig 4.15](#), a potential wire is shown surrounded by large amounts of aggregates in the bottom picture. This wire is in the centre of the image and is $0.1 \mu\text{m}$ in diameter with a length of which $2\mu\text{m}$ can be seen. The aggregate material is

similar in dimensions. A large sheet of material is seen in the bottom right of the image. In contrast, in Fig 4.16, the washed sample shows distinct wires. The top image shows wires 100-500 μm in length and 1-10 μm in diameter. There is a low density of spherical aggregates at 1-10 μm in diameter. At a higher resolution, these wires are seen to be stacks of wires 100nm in diameter. At this magnification, it is not possible to see whether nano-onions have bonded with the polymer and the fibres look featureless.



Figure 4.12: Sonicated nano-onions



Figure 4.13: The inclusion complex dissolved in DMF



Figure 4.14: Layers of the composite product

4.3.4 Discussion

Melting of the vessel occurred due because the DMF used for washing is corrosive. This material may effect the nervous system and damage the liver and kidneys so must be cleaned from the nanowires before use in a biological environment [38].

Samal et al used a mixture of FTIR, NMR and DLS to identify their composite [36]. A later paper used SEM on a similar dimer form and distinct spherical units were seen[36]. Spherical bumps to indicate the presence of nano-onions were not seen in Fig 4.16. The wires observed are probably constructed of multiple crosslinked polymeric chains with the magnification used too low to resolve individual nano necklaces. It is possible the onions were discarded during the washing stage and not added to the inclusion complex. Spectral analysis may determine their chemical presence or using a different imaging technique such as Transmission Electron Microscopy.

The chemistry behind this nanowire candidate came from a structural outlook. Linker chemistry was required to attach nano-onions to make a wire. The Buckminster fullerene paper [36] and follow up reviews [39] offer no electrical application or discuss the conductive properties of the system. The merits of a high-aspect conductive filler are for when the filler bulk is conductive, not partially conductive [22, 23]. It is unclear that connecting onions with non-conductive linkers benefit the conductivity of the polymer. Oxydianiline and cyclodextrin are not conductive molecules and their presence may hinder percolation through the conduit by increasing the mean distance between onions and preventing the

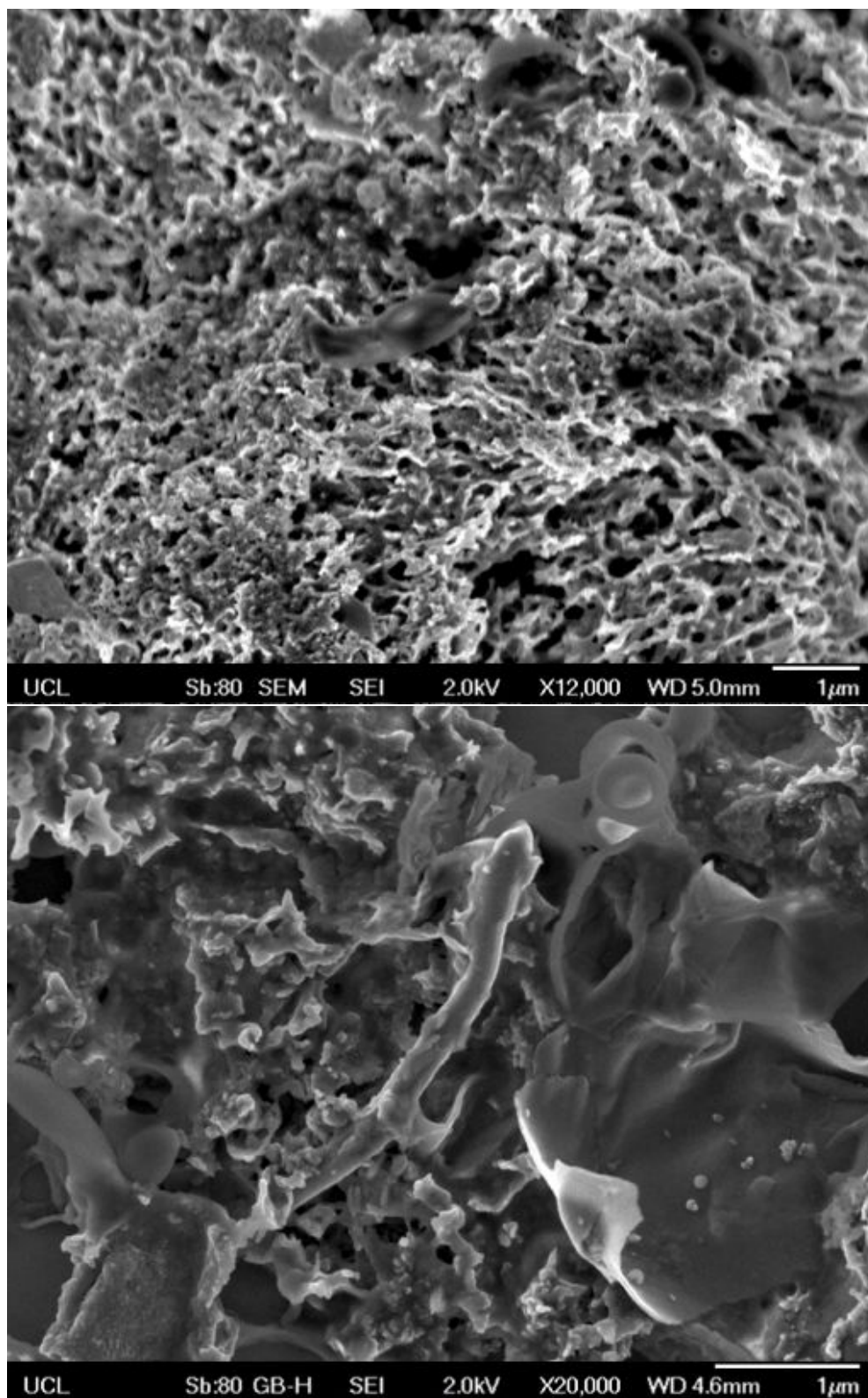


Figure 4.15: SEM images of the unwashed sample.

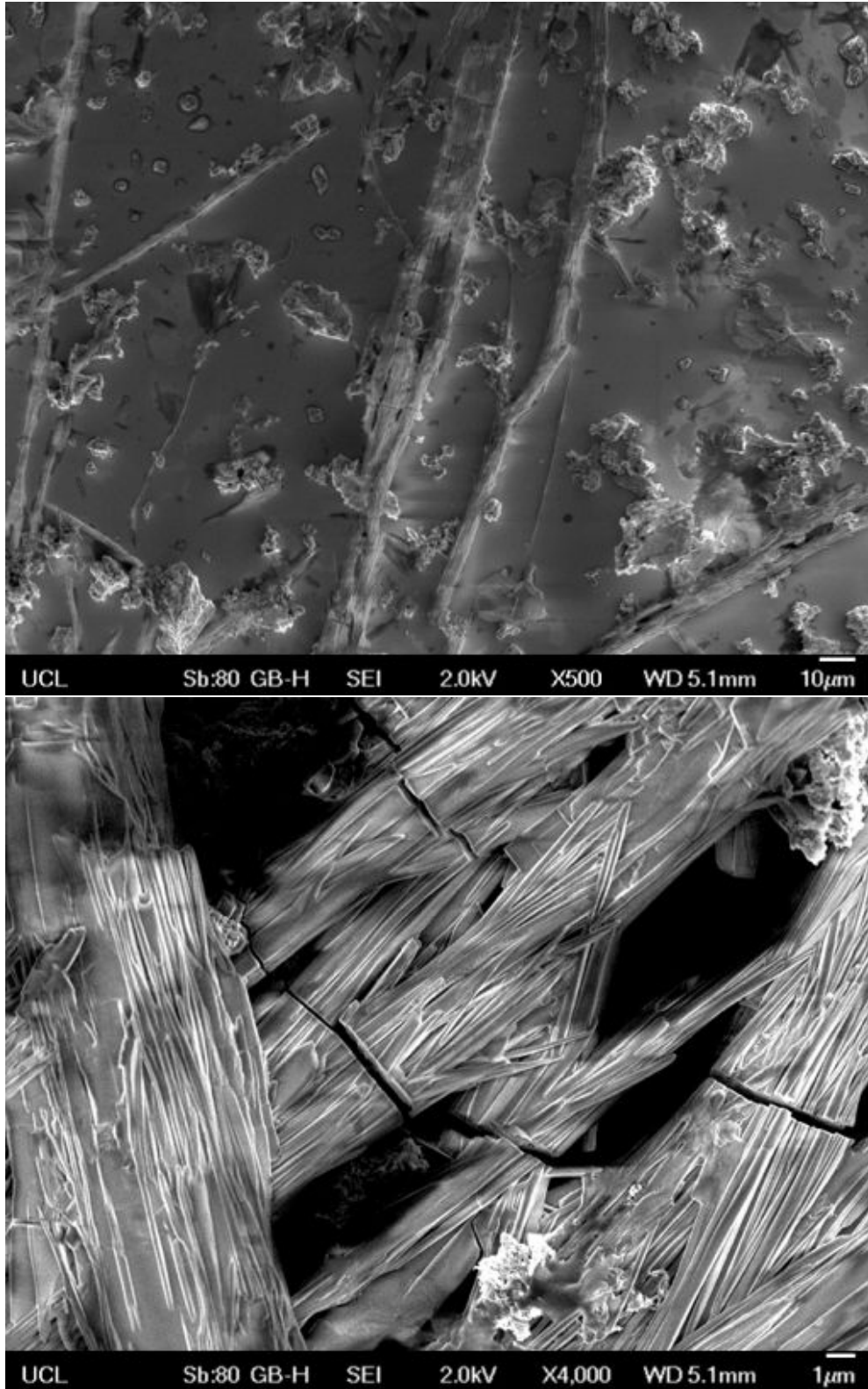


Figure 4.16: SEM images of the washed sample

formation of conducting clusters. Further work will look to a nanowire candidate where the bulk is conductive.

As the initial nanoparticles were not conductive, there is no reason to suggest the wires are so no electrical measurements were performed. There is further trouble producing new nano-onions in the laboratory so the adoption of a new nanoparticle will be considered.

Chapter 5

Graphene decorated Polyaniline

5.1 Initial Interfacial Polymerisation of Aniline

5.1.1 Overview

Polyaniline (pAni) is the best researched conductive electroactive polymer owing to its ease of synthesis. Before, complicated templating techniques were required. This has been superseded by a facile interfacial polymerisation [40]. Next to new synthesis techniques, the greatest research area has been characterising these electroconductive mechanisms [41]. The polymer has conductive properties in half-oxidised emeraldine form when doped, forming a polaron lattice [42]. Here the conductivity of the polymer increases by an order of 10^{10} to 1Scm^{-1} [43]. A polaron is the name given to an electron surrounded by a polarisation field [44]. The electron polarises the molecule, which acts back on the electron, reducing its effective mass. As the electron diffuses along the polymer, this field follows it [45]. The size of the polaron is defined by the extent of the surrounding polarisation field. In the mid 1990s, water soluble forms were derived[46]. Recent research focuses on the production of nanofibres. Luo et al published a facile synthesis for a composite with good aqueous dispersibility and electrical conductivity three orders of magnitude higher than that of single pAni fibre when added to a bulk graphene substrate[47].

Polymerisation from aniline will be undertaken to produce pAni nanofibres. The initial proposal is to then add a sonicated sample of graphene flakes to the

synthesised nanofibres under low heat, and analyse attachment in the same way as a paper on silica nanoparticles [48]. It is proposed the nanocomposite will be degraded in a physiological environment via hydrolysis with the graphene nanoparticles leaving the body through the bloodstream [24]. The justification for following an alternative route as opposed to improving the nano onion necklace is that this new strategy has a strong conduction mechanism. Poor nano onion conductivity was evidenced in the first chapter and the laboratory is currently unable to produce further material. In the literature, nano onions show promising candidate for supercapacitors but not as better conductive or biocompatible nanoparticles than graphene [30]. Graphene flakes are simpler molecules: they are fragments of graphene of the order $\sim 1-100\text{nm}$ [49]. Graphene is a single layer of sp^2 bonded carbon atoms packed in a dense honeycomb structure. It has been synthesised in water soluble forms [50] and shown to exhibit extremely high electron mobility [51, 52]. PAni, although exhibiting metal conductivity with the polaron mechanism mentioned, is thought to be mainly amorphous due to random chain conformations and chemical defects. Long range electron hopping occurs between crystalline islands [41]. On adding graphene flakes, attraction between the aromatic rings of each molecule causes the graphene to stack face-centred on top of the pAni [53]. It has been proposed that the adhesion of a large planar molecule will make pAni more rigid and ordered, improving the conducting pathway along the polymer backbone [6, 54, 55, 56, 57].

5.1.2 Experimental Procedure

5.1g of aniline monomer was dissolved in a beaker of 150ml toluene. In another beaker, dodecylbenzene sulfonic acid was dispersed in 150ml distilled water together with 12.5g ammonium persulphate. After magnetic stirring for one hour, the initial solution is transferred carefully into the second without disturbing the interface. Then, the reaction system was kept in a refrigerator (4°C) for 24 hours without disturbance. The upper oil part of the system was removed using a syringe. The lower aqueous phase was washed/centrifuged several times with deionised water in an attempt to retrieve solid pAni.

5.1.3 Results

The reaction system is shown in Fig 5.1. Clear layers are observed. On centrifuge, nil solid product was retrieved. The solution in the tube remained liquid and did not pelletise as experienced with previous centrifuge treatments.



Figure 5.1: The interfacial polymerisation reaction system

5.1.4 Discussion

Liu et al give the aniline reactant in grams [58]. The Department Safety Officer recommended solid aniline is used as liquid and vapour forms are highly hazardous. It was considered the reason solid pAni was not retrieved was because the aniline used was in liquid form. The purchase of solid aniline was attempted but it was discovered it does not exist for the species has a melting point of -6.3°C [59]. Future research will look for a different dopant acid. Many alternatives are discussed in a thorough review paper [40]. HCl would be most suitable as it provides the smallest diameter fibres at 30nm.

5.2 Graphene Oxide and Polyaniline

5.2.1 Overview

Further literature research uncovered Graphene Oxide (GO) addition to pAni had been achieved successfully by Wang et al with applications for supercapacitors [60]. Following the failure of the previous method, it was agreed that a suitable step would be to replicate these results. The use of graphene terminated with oxygen groups is justified as electrostatic interactions with oxygen ions and hydrogen bonding with the hydroxyl groups should provide a better bound composite [6]. A proposed attachment mechanism is shown in Fig 5.2.

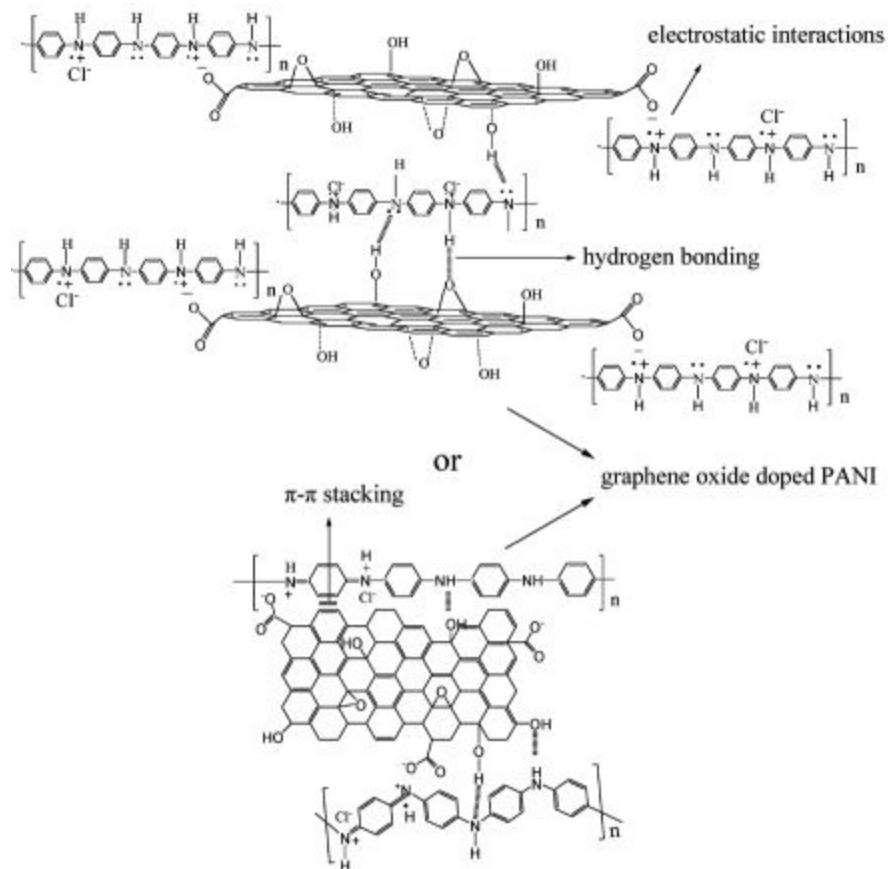


Figure 5.2: Attachment between graphene oxide and polyaniline from [6]

The flakes must first be oxidised to add the functional groups required. The development of Hummers method by Marcano et al [61] has been well adopted

in the literature. The method detailed in Zhang et al was used for convenience, as the product can be left to mix for 24 hours [62]. It was decided that an initial mass ratio of 1:1 GO flakes would be added to aniline before polymerisation. One key modification to the paper was made. Instead of the complicated freeze-drying procedure recommended in the paper, vacuum drying of the graphite oxide was adopted as carried out in the onion necklace work.

5.2.2 Experimental Procedure

A 9:1 mixture of concentrated $\text{H}_2\text{SO}_4/\text{H}_3\text{PO}_4$ (45:5 mL) was added to 0.375g of graphite flakes mixed with 2.25g of KMnO_4 . The reaction was heated to 50°C and mechanically stirred for 24 hours. The reaction was cooled to room temperature and poured onto 200ml of ice with 30% H_2O_2 (3 mL). After this, the mixture was centrifuged at 8000 rpm for 5 minutes. The remaining solid material was washed in succession with 200 mL of 30% HCl for two times, and 200 mL of water for three times. For each wash, the mixture was centrifuged at 13000 rpm for 20 minutes and the remaining product kept. The final product was dried in a vacuum chamber for 24 hours to obtain graphite oxide. Graphite oxide was further diluted in deionized water and sonicated for 60 minutes to obtain GO.

5ml of aniline was added into an aqueous solution of graphite oxide with a mass ratio of 1:1. The mixture was sonicated for an hour. Then the chemical polymerisation was performed by the slow addition of H_2O_2 (6 mL, 30%), hydrochloric acid (4.5 mL, 37%), and 0.1 mol/L $\text{FeCl}_3 \cdot 6\text{H}_2\text{O}$ (1 mL) under violent mechanical stirring to form a 200 mL solution. The suspension was stirred in an ice bath for 24 hours. The final product was filtered and washed with excess of HCL and acetone. Finally, the material was dried in a vacuum chamber for 24 hours. Then, the composite was characterised using SEM and EIS as used in the previous chapter.

5.2.3 Results

Fig 5.3 shows the brown suspension formed by the flakes after stirring for 24 hours. On adding H_2O_2 , the liquid turned a bright yellow (see Fig 5.4). Fig 5.5 shows the crisp flake-like texture of the dried product. Fig 5.6 shows the

sonication of GO and aniline. The GO was soluble in water. The suspension, as kept in the ice bath for 24 hours, is shown in Fig 5.7. The filtration process is shown in Fig 5.8.

In Fig 5.9, SEM on the vacuum dried pAni-GO composite exhibited occasional fibrous areas as seen in the top image. These fibres are tangled and have a diameter of 100nm. However, the product is mostly aggregated as the bottom image shows with hard 1 μ m flakes the dominant feature. EIS is carried out on the product at a range of temperatures. The results are shown in Fig 5.10. This can be seen by the radius of the real against imaginary impedance axis component that as the temperature increases, the resistivity of the product increases. At all temperatures, the material displays a high pass characteristic with high frequency signals showing a low impedance.



Figure 5.3: The oxidation solution

5.2.4 Discussion

Chen et al report the formation of a bright yellow suspension on adding H₂O₂ as found in Fig 5.4 [63]. The dried GO was water soluble as found by Wang et al [6] (see Fig 5.6).

Wang et al [6] undergo EIS on their composites. From the Cole-Cole plots, they show the composite performs better than its components. They show a



Figure 5.4: After the addition of H₂O₂



Figure 5.5: Graphite oxide



Figure 5.6: Suspension of graphene oxide in aniline



Figure 5.7: pAni-GO composite stirred under ice bath



Figure 5.8: The filtered pAni-GO composite

GO:pAni 100:1 ratio has a better electrochemical capacitance than 61:1 although a similar resistance. Their resistances are lower with semicircles around 200Ω in diameter. A similar result is given by Zhang et al [57] suggesting space for improvement with this technique however the bulk conductance is a better metric and will be calculated in further analysis using an appropriate equivalent circuit. Also, in the next section, a trend between the resistivity and temperature will be explored.

A highly agglomerated sample is observed through SEM in Fig 5.9. Wang et al [6] notice mainly unregular morphology including agglomeration with a 1:23 ratio. In contrast, they see a 300nm diameter fibre morphology at 1:100 with these large fibres built from smaller nanofibres about 30 nm in diameter and 100-150 nm in length. The next stage will be to adjust our 1:1 ratio to 1:100 and reassess physical properties. Wang et al notes changing the ratio may greatly affect the electrochemical performance. This shall be explored.

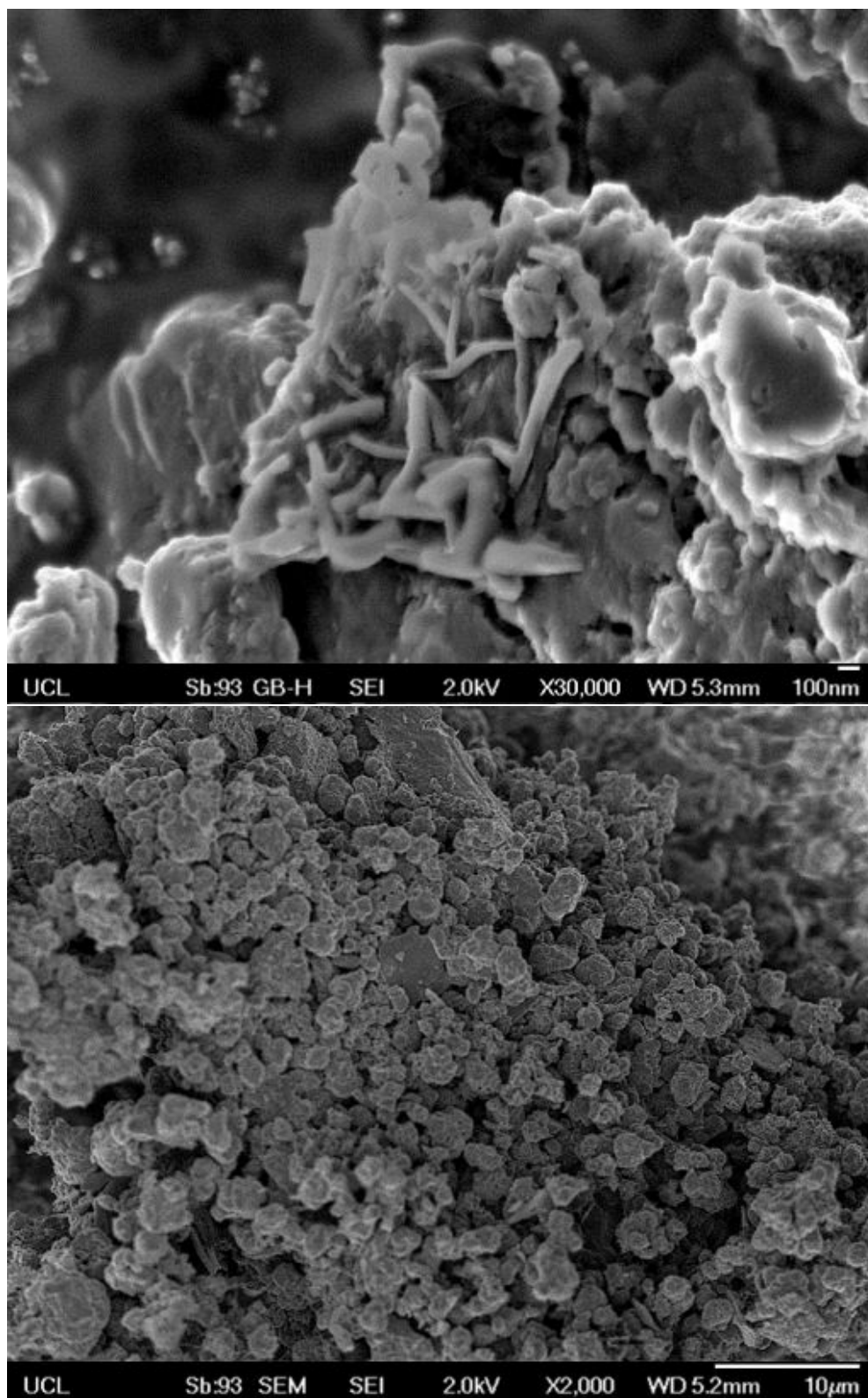


Figure 5.9: SEM on the pAni-GO

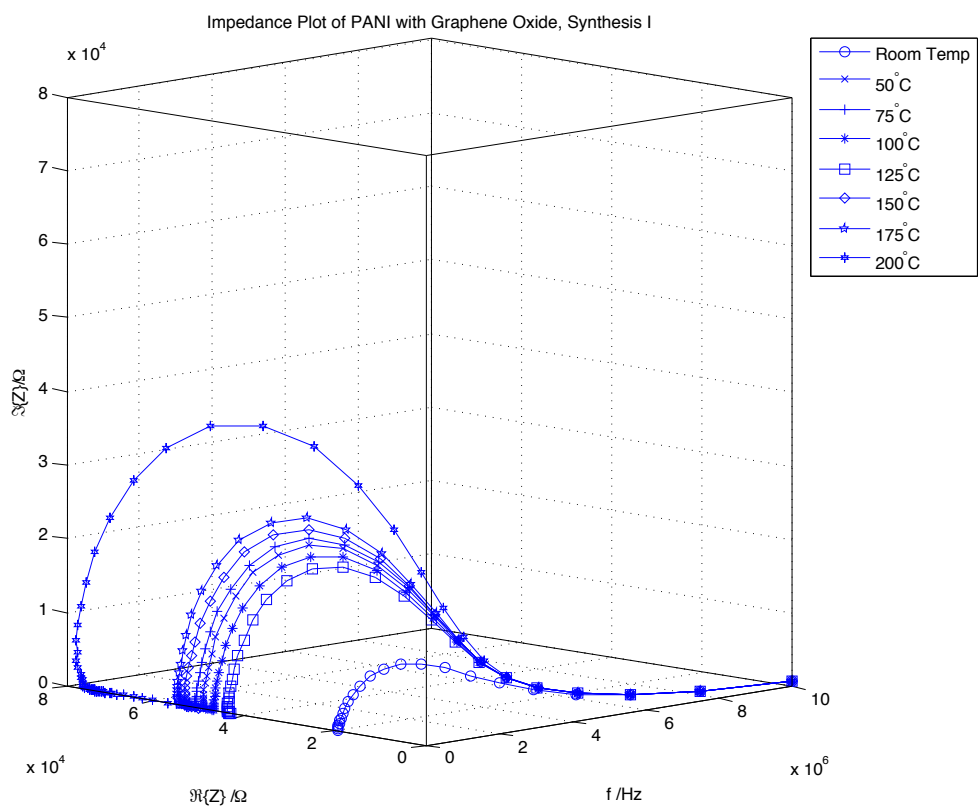


Figure 5.10: Electrochemical Impedance Spectroscopy on the pAni-GO

5.3 Modifications and Further Analysis

5.3.1 Overview

Judging from SEM, most product in our first synthesis is aggregated and not wire-like. This could be because our ratio of graphene to pAni is too high. Two orders of magnitude less, 1:100, will be used as with Wang et al [6] to see if the fibrous morphology they report is observed. Additionally, the oxidised graphene flakes could be too large and overwhelm the pAni fibres. AFM should indicate the diameter of single flakes. Ball milling may be required to process them to the nanoscale [49].

5.3.2 Results

The fibre synthesis was repeated with the ratio changed to 1:100 GO to pAni. SEM shows a different morphology to before. The product is mostly sheet like. The aggregated bulk appears less firm than Fig 5.9, taking on a more wooly texture to the discrete stones seen previously.

EIS was repeated on this sample for different temperatures, as shown in Fig 5.14. We compare the resistance taken at 50° for each synthesis. Fitting a circular plot in Fig 5.15, it is seen that the resistance is much increased from 49605Ω in the first synthesis to 350230Ω. Surprisingly, the radius of the circles in Fig 5.14 decreases with temperature in this plot whereas it increased with temperature with the previous ratio (see Fig 5.10). A circle fit was systematically taken at each measurement and temperature plot was constructed in Fig 5.16. Two distinct trends are shown. The 1:100 ratio is plotted for Mott Variable Range Hopping in Fig 5.17 with a good correlation. The 1:1 ratio is quadratically fit for graphene in Fig 5.18 with less perfect results.

AFM was performed on a sample of graphene oxide. A piece of Czochralski silicon was initially twice cleaned by ultrasound for 15 min in ethanol, and once for 15 min in CH₂Cl₂. It was then rinsed in water four times and left for 30 minutes in water. The flakes were oxidised using the method detailed earlier, dissolved in water, and sonicated into the wafer piece. Fig 5.11 shows what is expected to be a flake. It is 0.5μm in diameter. However, the surface was

uneven. Fig 5.12 shows craters larger than the flake feature size that made GO flakes harder to verify. The observed flake may be a silicon surface defect. It was difficult to produce a series of good quality images using this technique due to high noise levels, as noted in Chapter 4. This single flake observation does not provide strong evidence.

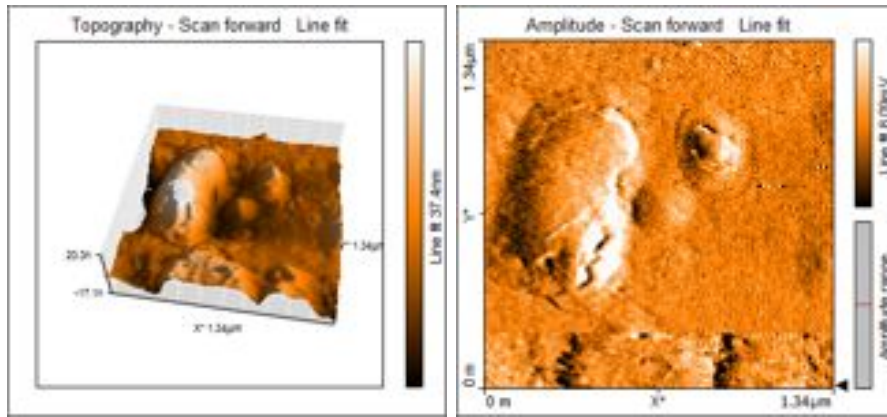


Figure 5.11: AFM of graphene oxide

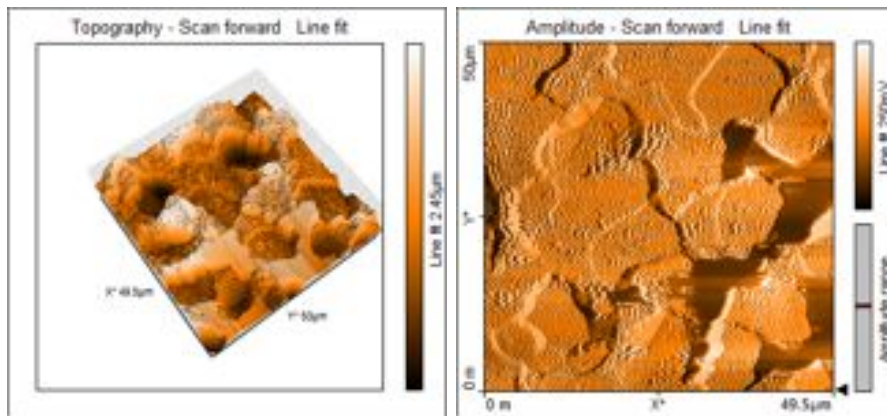


Figure 5.12: The surface was uneven and porous in places

5.3.3 Discussion

SEM showed the wire structure was not achieved although the morphology is more fibrous. Zhang et al report a similar image[57]. They attribute the sheet-like constituent to large graphene flakes.

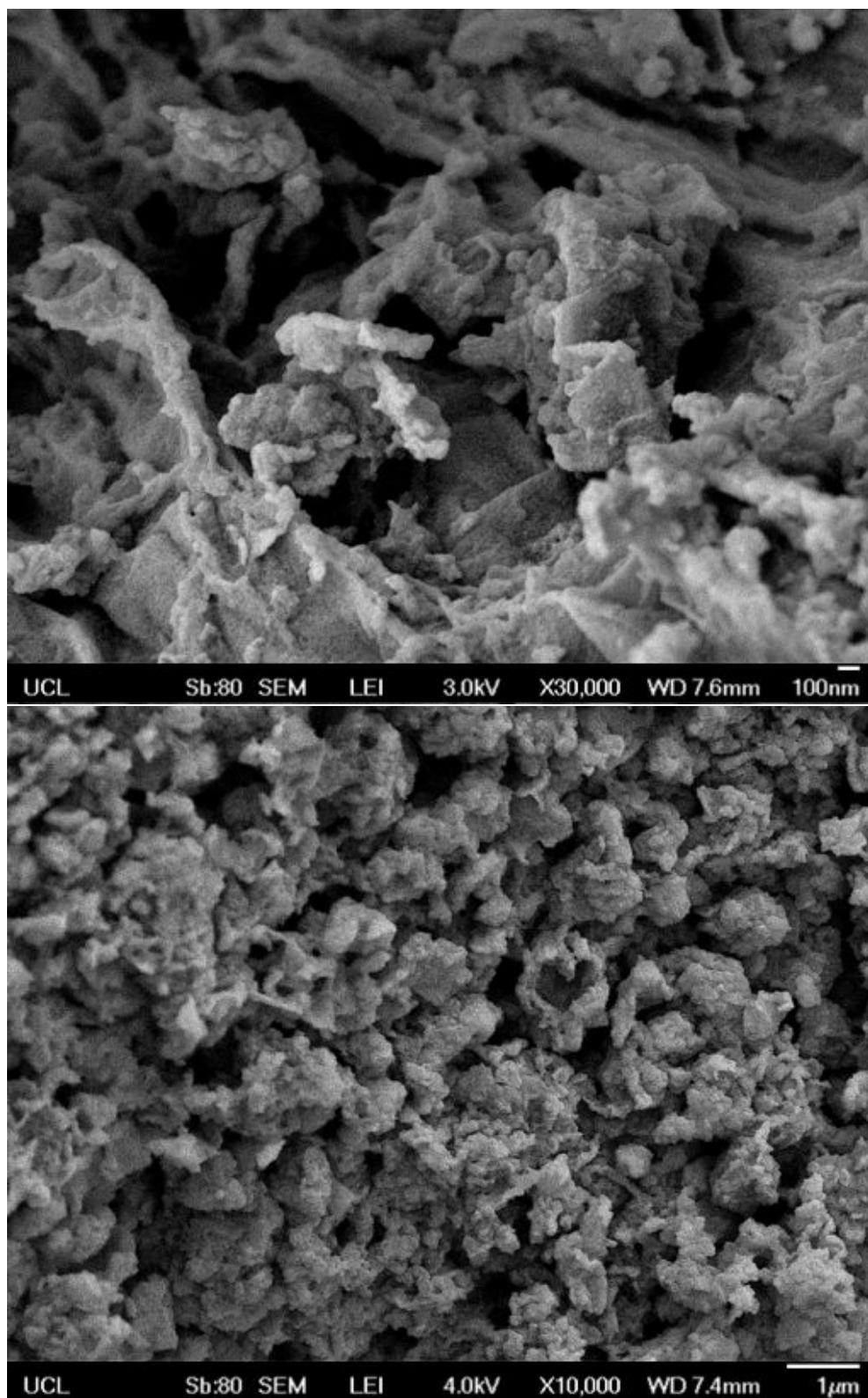


Figure 5.13: SEM on the second pAni-GO synthesis

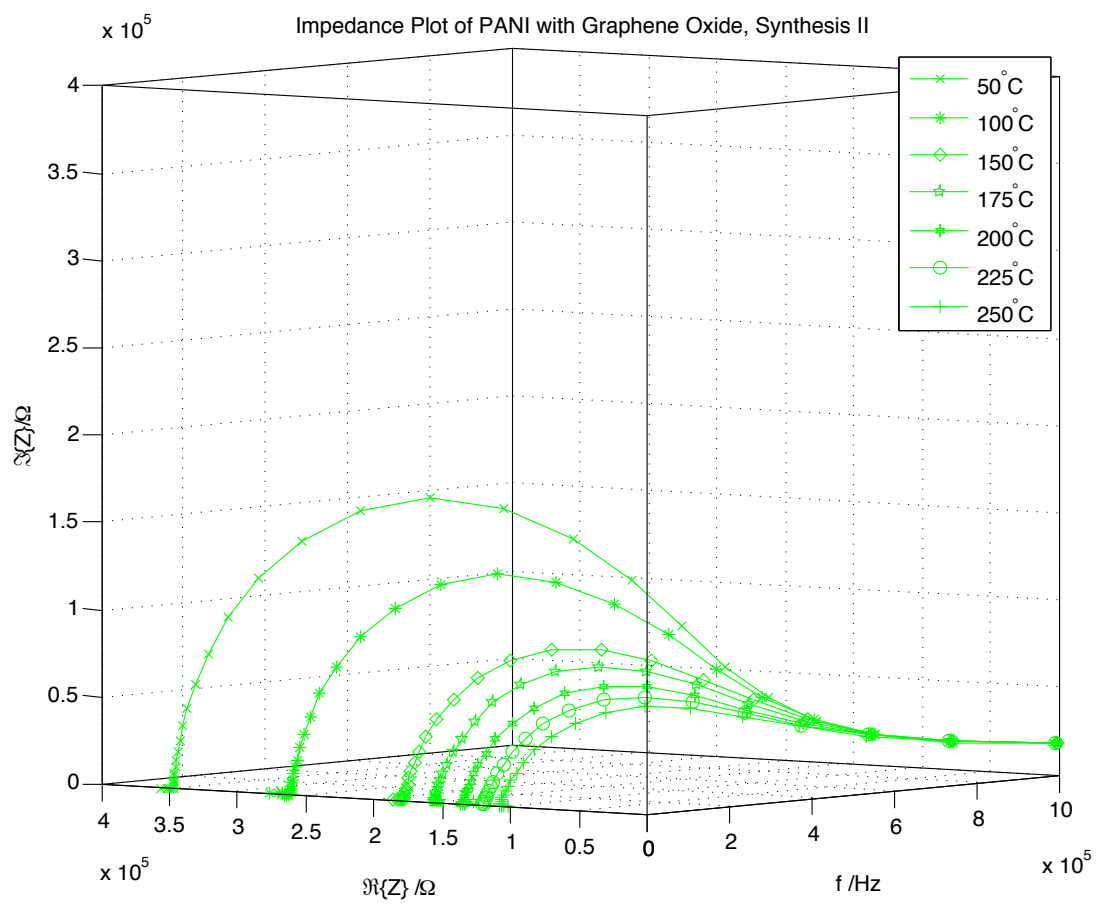


Figure 5.14: EIS on the second synthesis

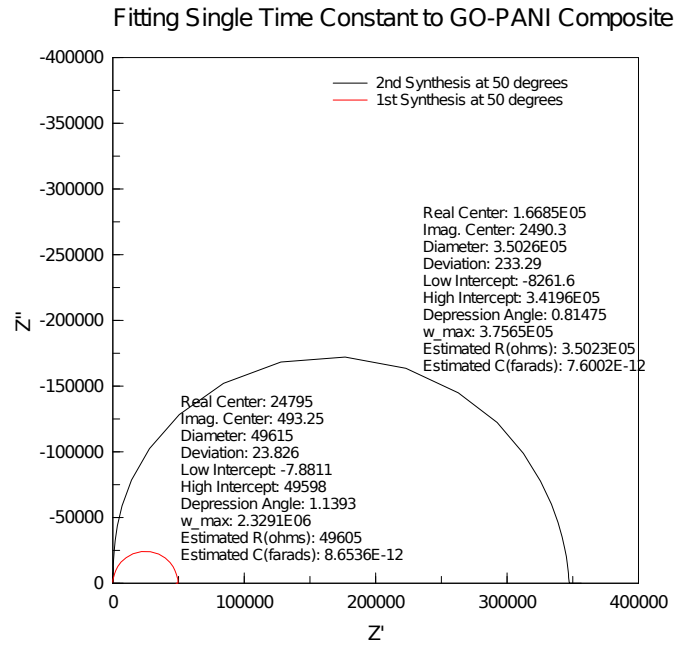


Figure 5.15: The second synthesis shows a much higher resistivity than before

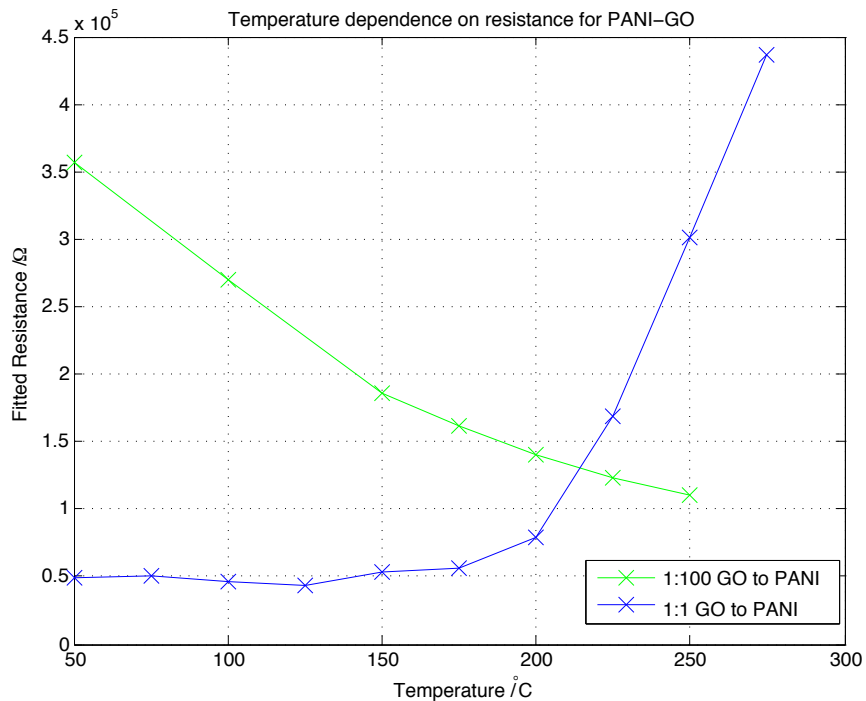


Figure 5.16: Resistance plotted against temperature shows distinct trends for the two ratios

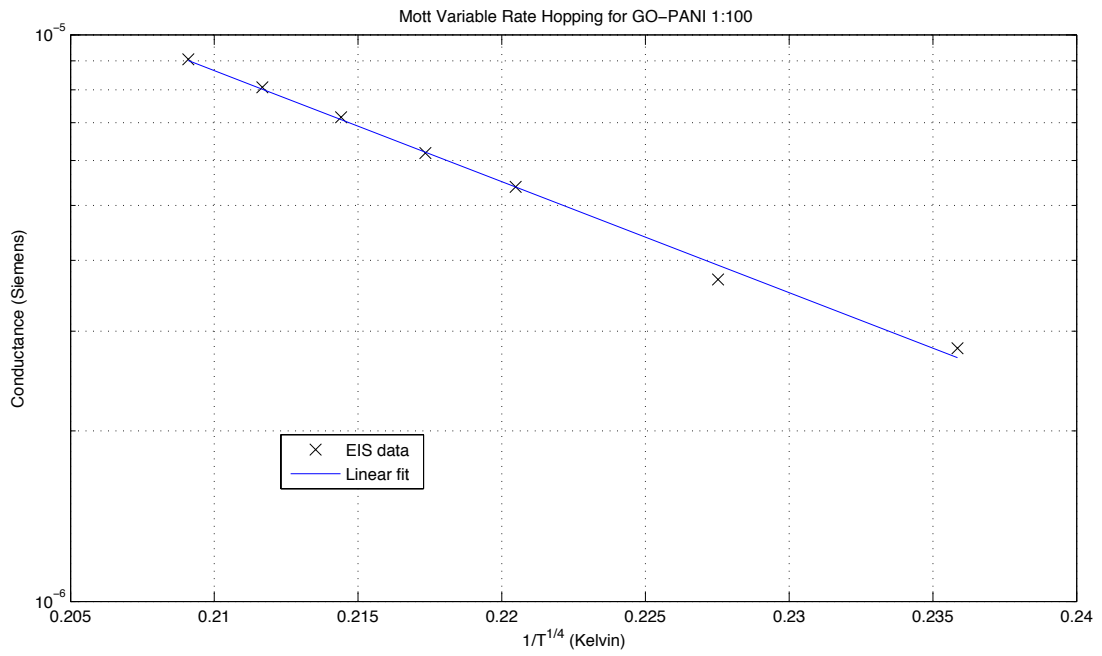


Figure 5.17: 1:100 PANi-GO with Mott Variable Hopping Fit

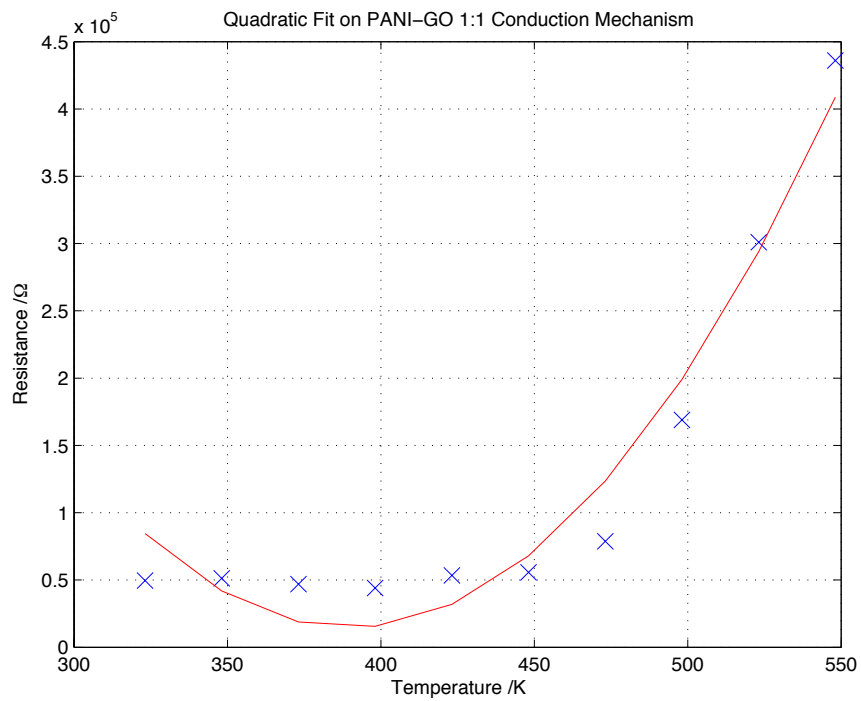


Figure 5.18: 1:1 PANi-GO with quadratic temperature fit

Chen et al [63] perform AFM on GO flakes. These images show sharp flake boundaries and not the round morphology seen here. Several flakes overlap. However, the features are the same diameter at $0.5\mu\text{m}$. In this paper, GO was deposited on freshly cleaved surfaces to better avoid defects. Marcano et al [61] show a shard-like flake again with a $0.5\mu\text{m}$ profile.

PAni-GO will have several resistive and capacitive conduction pathways. As a first order approximation, the same single time constant model was used as the onions in fitting the resistance values of Fig 5.15. Marins et al [64] assert a bulk conductivity to their pAni composite from the EIS measurements using Eq 5.1.

$$\sigma = \frac{\ell}{R \cdot A} \quad (5.1)$$

The length between the EIS probes was $1 \pm 0.5\text{cm}$ and the area of the sample is approximately $1 \pm 0.5\text{mm} \times 1 \pm 0.5\text{mm}$. Eq 5.3 gives values that are very approximate due to the lack of accuracy in measuring these distances. However, these values are the same order of magnitude as the 1 S cm^{-1} known in the literature for doped PAni [43].

$$\sigma_{1:1} = 63 \pm 58 \text{ S cm}^{-1} \quad (5.2)$$

$$\sigma_{1:100} = 8.9 \pm 8.2 \text{ S cm}^{-1} \quad (5.3)$$

Fig 5.16 is important because it shows the composite observes an entirely different conduction mechanism when saturated with graphene. Mott variable range hopping is used to characterise the conductivity of non-crystalline semiconductors like pAni. The material has a low mobility due to the polaron mechanism detailed previously and hopping occurs over amorphous regions between metallic sites where the probability of hopping is given, in the 3D case, by $(\frac{T_0}{T})^{1/4}$ [65] providing a conductivity given in Eq 5.4. Stallinga [66] offers an excellent primer showing hopping to be an extension of the percolation between conductive sites detailed in Chapter 2.

$$\sigma = \sigma_0 \exp -\left(\frac{T_0}{T}\right)^{1/4} \quad (5.4)$$

Rearranging, we will see a linear trend for conductance G

$$\ln G = -\left(\frac{T_0}{T}\right)^{1/4} + c \quad (5.5)$$

Campos et al show this trend fitting in pAni for a large temperature range [67]. We show this trend fits well for our 1:100 sample in Fig 5.17. To explain the trend in the 1:1 ratio, we look to conduction in graphene as the dominant term. Research shows monolayer graphene displays a quadratic temperature-resistivity relation due to scattering of electrons by out-of-plane phonons (termed *flexural*) [68, 69].

$$\rho \sim T^2 \quad (5.6)$$

We fit a quadratic to our data set and show a weak correlation (see Fig 5.18) due to an initial flattening of the curve. The low temperature points look linear. Ochoa et al [70] observe an experimental logarithmic correction results in initial flattening.

$$\rho \sim T^2 \ln T \quad (5.7)$$

Schiefele et al report a flattening of the quadratic when interfaced with SiO₂ and even more so with boron nitride due to surface phonons at the substrate [71]. In contrast, an established theoretical framework uses Boltzman's transport equation to fit an exponential temperature dependence [72].

$$\rho \propto \exp T \quad (5.8)$$

None of these models fit well. Establishing a justified theoretical model for polyaniline and graphene/graphene oxide interactions is beyond the scope of this paper. It is important to note the metallic characteristic of this trend however (resistivity increases with temperature) and further data should be collected to establish this relation.

5.4 Polyaniline Nanofibres

5.4.1 Overview

It is clear from SEM images in the previous section that, unlike the nano-necklace, distinct nanowires have not been achieved here. This second strategy, although providing better electrical conductivity has thus far evidenced to be a weaker structural candidate. In this final experiment, pAni will be synthesised without the GO flakes to observe, by SEM, the change in morphology the GO flakes introduce. It is assumed that the polymerisation of aniline in isolation will produced good fibrous material.

5.4.2 Experimental Procedures

To 5ml of aniline, the chemical polymerisation was performed by the slow addition of H_2O_2 (6 mL, 30%), hydrochloric acid (4.5 mL, 37%), and 0.1 mol/L $\text{FeCl}_3 \cdot 6\text{H}_2\text{O}$ (1 mL) under violent mechanical stirring to form a 200 mL solution.

5.4.3 Results

Fig 5.19 shows bright distinct cobweb fibres in the top image surrounded by bulbous material. These fibres are around 20nm in diameter and 400nm in length. The bottom image shows a central section where the fibrous material is around 100nm in diameter surrounded by more agglomerated material.

5.4.4 Discussion

The thicker wires in the bottom picture of Fig 5.19 are probably constructed from several of the top nanofibres. These pictures clearly show the problem with the morphology of the nanocomposite lies with the polymerisation of aniline. Large areas of agglomeration contrast with the distinct fibres shown in Fig 4.16 of the original synthesis. In future, studying the review paper of Huang [40], different dopants will be attempted and this technique refined.

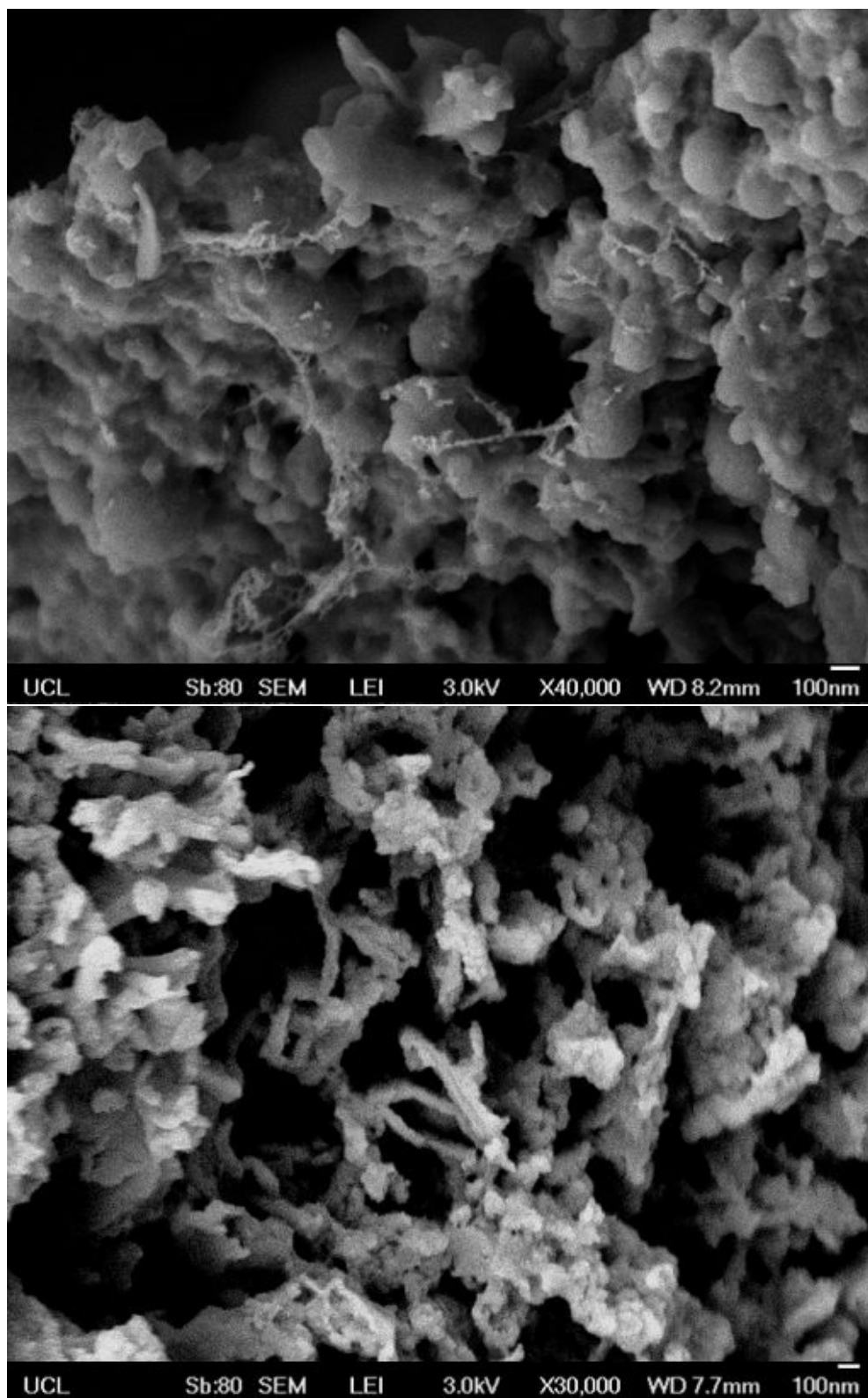


Figure 5.19: SEM on pAni

Chapter 6

Conclusions

In this project, two unique biodegradable nanowire composites have been designed and synthesised using a collaboration of nanoparticles and polymeric technology. Overall, it has been shown that these novel composites have structural and electrically conductive promise for use as a nanowire in a biological context.

In Chapter 4, a biodegradable wire structure, termed a nano-necklace, was developed using nano onions linked together by an inclusion complex. The inclusion complex was synthesised and verified using FTIR analysis as the product shared spectral peaks with the two reactants. The nano onions were added and, after centrifuge washing, SEM showed a promising structural candidate for nanowires. The current nano onion sample did not display conductive properties but future onions, when surface terminated or grown under different conditions will display good conductive properties and there is future work to electrically characterise this device.

In Chapter 5, a new wire was designed by interfacing graphene oxide on polyaniline to improve the conductive properties of the wire through pi- stacking of flakes along the polymeric backbone. The most exciting result was to observe the conduction mechanism adopting a metallic temperature-dependent trend on saturating with graphene. A strong correlation to the Mott variable hopping rate theory was shown for low graphene doping. At high concentration, the material showed a good electrical conductivity of the order 10 S cm^{-1} .

Looking forwards, it will be necessary to improve upon the wire quality of the second candidate by modification of the polymerisation chemistry. This will

require time and chemical expertise. A paper published this year looks to wrap graphene on pre-polymerised polyaniline nanofibres [73]. This may be a good strategy to separate polymer chemistry from nanocompositing and avoid graphene interfering at the polymerisation stage. It would be important to extract a single nanowire and perform electrochemical tests on it. Alternately, a single nanofibre can be grown electrochemically with nanoparticles added later [74]. This may be a valid research direction. The real test would be to observe the effects of this nanocomposite in situ. First, polyaniline should be added to the nerve conduit polymer and electrochemical tests performed before deploying the nanostructured composite.

In lieu of the results obtained, there is a viable strategy in using a nanowire to provide conduit conductivity. Research is required to optimise the properties of these devices but eventual deployment can bring the benefits of high-aspect fillers into a biological surrounding to affordably deliver good neural regrowth.

References

- [1] JD Enderle and JD Bronzino. *Introduction to Biomedical Engineering*. 2011. ISBN 9780123749796. URL <http://books.google.com/books?hl=en&lr=&id=twc-GL0t10QC&oi=fnd&pg=PP2&dq=Introduction+to+Biomedical+Engineering&ots=PGxWKixmaB&sig=SDEM0hD9X2vCcnPNj5xxf09hhHA>. iv, 3
- [2] Christine E Schmidt and Jennie Baier Leach. Neural tissue engineering: strategies for repair and regeneration. *Annual review of biomedical engineering*, 5:293–347, January 2003. ISSN 1523-9829. doi: 10.1146/annurev.bioeng.5.011303.120731. URL <http://www.ncbi.nlm.nih.gov/pubmed/14527315>. iv, 3, 4
- [3] Amit Pabari, Shi Yu Yang, Alexander M Seifalian, and Ash Mosahebi. Modern surgical management of peripheral nerve gap. *Journal of plastic, reconstructive & aesthetic surgery : JPRAS*, 63(12):1941–8, December 2010. ISSN 1878-0539. doi: 10.1016/j.bjps.2009.12.010. URL <http://www.ncbi.nlm.nih.gov/pubmed/20061198>. iv, 2, 3, 5
- [4] William D Callister. *Fundamentals of Materials Science and Engineering*. John Wiley & Sons, 5th edition, 2001. ISBN 047139551X. iv, 5
- [5] Liying Wang, Sudjit Luanpitpong, Vincent Castranova, William Tse, Yongju Lu, Varisa Pongrakhananon, and Yon Rojanasakul. Carbon nanotubes induce malignant transformation and tumorigenesis of human lung epithelial cells. *Nano letters*, 11(7):2796–803, July 2011. ISSN 1530-6992. doi: 10.1021/nl2011214. URL <http://www.pubmedcentral.nih.gov/articlerender.fcgi?artid=3135732&tool=pmcentrez&rendertype=abstract>. iv, 5

-
- [6] Hualan Wang, Qingli Hao, Xujie Yang, Lude Lu, and Xin Wang. Effect of graphene oxide on the properties of its composite with polyaniline. *ACS applied materials & interfaces*, 2(3):821–8, March 2010. ISSN 1944-8244. doi: 10.1021/am900815k. URL <http://www.ncbi.nlm.nih.gov/pubmed/20356287>. v, 29, 31, 33, 36, 39
- [7] Bryan J Pfister, Tessa Gordon, Joseph R Loverde, Arshneel S Kochar, Susan E Mackinnon, and D Kacy Cullen. Biomedical engineering strategies for peripheral nerve repair: surgical applications, state of the art, and future challenges. *Critical reviews in biomedical engineering*, 39(2):81–124, January 2011. ISSN 0278-940X. URL <http://www.ncbi.nlm.nih.gov/pubmed/21488817>. 2, 3
- [8] J Noble and CA Munro. Analysis of upper and lower extremity peripheral nerve injuries in a population of patients with multiple injuries. *The Journal of trauma*, 1998. URL http://journals.lww.com/jtrauma/Abstract/1998/07000/Analysis_of_Upper_and_Lower_Extremity_Peripheral.25.aspx. 2
- [9] A Waller. section of the glossopharyngeal and hypoglossal nerves of the frog, and observations of the alterations produced thereby in the structure of their primitive fibres. *Philosophical Transactions of the Royal Society of ...*, 140(1850):423–429, 1850. URL <http://onlinelibrary.wiley.com/doi/10.1002/cbdv.200490137/abstract><http://www.jstor.org/stable/10.2307/108444>. 2
- [10] R B Donoff. Nerve regeneration: basic and applied aspects. *Critical reviews in oral biology and medicine : an official publication of the American Association of Oral Biologists*, 6(1):18–24, January 1995. ISSN 1045-4411. URL <http://www.ncbi.nlm.nih.gov/pubmed/7632865>. 2
- [11] S Y Fu and T Gordon. The cellular and molecular basis of peripheral nerve regeneration. *Molecular neurobiology*, 14(1-2):67–116, 1997. ISSN 0893-7648. doi: 10.1007/BF02740621. URL <http://www.ncbi.nlm.nih.gov/pubmed/9170101>. 2

REFERENCES

- [12] Tina Sedaghati, Shi Yu Yang, Afshin Mosahebi, Mohammad S Alavijeh, and Alexander M Seifalian. Nerve regeneration with aid of nanotechnology and cellular engineering. *Biotechnology and applied biochemistry*, 58(5):288–300, 2011. ISSN 1470-8744. doi: 10.1002/bab.51. URL <http://www.ncbi.nlm.nih.gov/pubmed/21995532>. 2, 3
- [13] Jason S. Belkas, Molly S. Shoichet, and Rajiv Midha. Axonal guidance channels in peripheral nerve regeneration. *Operative Techniques in Orthopaedics*, 14(3):190–198, July 2004. ISSN 10486666. doi: 10.1053/j.oto.2004.06.001. URL <http://linkinghub.elsevier.com/retrieve/pii/S1048666604000436>. 2
- [14] Frank F a IJpma, Jean-Phillipe a Nicolai, and Marcel F Meek. Sural nerve donor-site morbidity: thirty-four years of follow-up. *Annals of plastic surgery*, 57(4):391–5, October 2006. ISSN 0148-7043. doi: 10.1097/01.sap.0000221963.66229.b6. URL <http://www.ncbi.nlm.nih.gov/pubmed/16998330>. 3
- [15] A SEIFALIAN, H SALACINSKI, and S HANCOCK. Polymer for use in conduits and medical devices. *WO Patent WO/2005/070,998*, 2005. URL <http://www.wipo.int/patentscope/search/en/WO2005070998>. 3
- [16] Joanne Raghunath, George Georgiou, David Armitage, Showan N Nazhat, Kevin M Sales, Peter E Butler, and Alexander M Seifalian. Degradation studies on biodegradable nanocomposite based on polycaprolactone/polycarbonate (80:20%) polyhedral oligomeric silsesquioxane. *Journal of biomedical materials research. Part A*, 91(3):834–44, December 2009. ISSN 1552-4965. doi: 10.1002/jbm.a.32335. URL <http://www.ncbi.nlm.nih.gov/pubmed/19051308>. 3
- [17] Ze Zhang, Mahmoud Rouabhia, Zhaoxu Wang, Christophe Roberge, Guixin Shi, Phillippe Roche, Jiangming Li, and Lê H Dao. Electrically conductive biodegradable polymer composite for nerve regeneration: electricity-stimulated neurite outgrowth and axon regeneration. *Artificial organs*, 31(1):13–22, January 2007. ISSN 0160-564X. doi: 10.1111/j.1525-1594.2007.00335.x. URL <http://www.ncbi.nlm.nih.gov/pubmed/17209956>. 3

REFERENCES

- [18] a. Battisti, a.a. Skordos, and I.K. Partridge. Percolation threshold of carbon nanotubes filled unsaturated polyesters. *Composites Science and Technology*, 70(4):633–637, April 2010. ISSN 02663538. doi: 10.1016/j.compscitech.2009.12.017. URL <http://linkinghub.elsevier.com/retrieve/pii/S0266353809004527>. 3
- [19] Armin Bunde and JW Kantelhardt. Diffusion and Conduction in Percolation Systems Theory and Applications. *uni-giessen.de*, pages 1–19, 2005. URL <http://www.uni-giessen.de/physik/theorie/theorie3/publications/JWK-Springer1.pdf>. 3
- [20] W Xia and MF Thorpe. Percolation properties of random ellipses. *Physical Review A*, 38(5):2650–2656, 1988. URL http://pra.aps.org/abstract/PRA/v38/i5/p2650_1. 4
- [21] L. Berhan and a. Sastry. Modeling percolation in high-aspect-ratio fiber systems. I. Soft-core versus hard-core models. *Physical Review E*, 75(4):041120, April 2007. ISSN 1539-3755. doi: 10.1103/PhysRevE.75.041120. URL <http://link.aps.org/doi/10.1103/PhysRevE.75.041120>. 4
- [22] M. Foygel, R. Morris, D. Anez, S. French, and V. Sobolev. Theoretical and computational studies of carbon nanotube composites and suspensions: Electrical and thermal conductivity. *Physical Review B*, 71(10):104201, March 2005. ISSN 1098-0121. doi: 10.1103/PhysRevB.71.104201. URL <http://link.aps.org/doi/10.1103/PhysRevB.71.104201>. 4, 24
- [23] Fangming Du, John Fischer, and Karen Winey. Effect of nanotube alignment on percolation conductivity in carbon nanotube/polymer composites. *Physical Review B*, 72(12):1–4, September 2005. ISSN 1098-0121. doi: 10.1103/PhysRevB.72.121404. URL <http://link.aps.org/doi/10.1103/PhysRevB.72.121404>. 4, 24
- [24] Hak Soo Choi, Wenhao Liu, Preeti Misra, Eiichi Tanaka, John P Zimmer, Binil Itty Ipe, Mounsi G Bawendi, and John V Frangioni. Renal clearance of quantum dots. *Nature biotechnology*, 25(10):1165–70, October 2007. ISSN 1087-0156. doi: 10.1038/nbt1340.

REFERENCES

- URL <http://www.pubmedcentral.nih.gov/articlerender.fcgi?artid=2702539&tool=pmcentrez&rendertype=abstract>. 5, 9, 17, 29
- [25] J. Macutkevic, D. Seliuta, G. Valusis, J. Banys, S. Hens, V. Borjanovic, V. Kuznetsov, and O. Shenderova. Effect of thermal treatment conditions on the properties of onion-like carbon based polymer composite. *Composites Science and Technology*, 70(16):2298 – 2303, 2010. ISSN 0266-3538. doi: 10.1016/j.compscitech.2010.09.008. URL <http://www.sciencedirect.com/science/article/pii/S0266353810003532>. Metal Matrix Composites Reinforced with Nano-sized Reinforcements. 7
- [26] L Hawelek, A Brodka, S Tomita, J C Dore, V Honkimäki, and A Burian. Diamond & Related Materials Transformation of nano-diamonds to carbon nano-onions studied by X-ray diffraction and molecular dynamics. *Diamond & Related Materials*, 20(10):1333–1339, 2011. ISSN 0925-9635. doi: 10.1016/j.diamond.2011.09.008. URL <http://dx.doi.org/10.1016/j.diamond.2011.09.008>. 9
- [27] Fu-Dong Han, Bin Yao, and Yu-Jun Bai. Preparation of Carbon Nano-Onions and Their Application as Anode Materials for Rechargeable Lithium-Ion Batteries. *The Journal of Physical Chemistry C*, 115(18):8923–8927, May 2011. ISSN 1932-7447. doi: 10.1021/jp2007599. URL <http://pubs.acs.org/doi/abs/10.1021/jp2007599>. 9
- [28] Chenguang Zhang, Jiajun Li, Chunsheng Shi, Enzuo Liu, Xiwen Du, Wei Feng, and Naiqin Zhao. The efficient synthesis of carbon nano-onions using chemical vapor deposition on an unsupported NiFe alloy catalyst. *Carbon*, 49(4):1151–1158, April 2011. ISSN 00086223. doi: 10.1016/j.carbon.2010.11.030. URL <http://linkinghub.elsevier.com/retrieve/pii/S0008622310008389>. 9
- [29] Joanna Luszczyn, Marta E Plonska-brzezinska, Amit Palkar, Alina T Dubis, Agneta Simionescu, Dan T Simionescu, Beata Kalska-szostko, Krzysztof Winkler, and Luis Echegoyen. Small Noncytotoxic Carbon Nano-Onions : First Covalent Functionalization with Biomolecules. *Chemistry: A European Journal*, pages 4870–4880, 2010. doi: 10.1002/chem.200903277. 9, 14, 16

REFERENCES

- [30] John K McDonough, Andrey I Frolov, Volker Presser, Junjie Niu, Christopher H Miller, Teresa Ubieto, Maxim V Fedorov, and Yury Gogotsi. Influence of the structure of carbon onions on their electrochemical performance in supercapacitor electrodes. *CARBON*, pages 1–12, 2012. ISSN 0008-6223. doi: 10.1016/j.carbon.2011.12.022. URL <http://dx.doi.org/10.1016/j.carbon.2011.12.022>. 9, 29
- [31] A I Romanenko, O B Anikeeva, V L Kuznetsov, T I Buryakov, E N Tkachev, S I Moseenkov, and A N Usoltseva. Influence of gases on conductivity of onion-like carbon and multiwalled carbon nanotubes. 10(7):1749–1753, 2008. 9, 14
- [32] J. Pironon, R. Thiery, M. Ayt Ougougdal, S. Teinturier, G. Beaudoin, and F. Walgenwitz. Ft-ir measurements of petroleum fluid inclusions: methane, n-alkanes and carbon dioxide quantitative analysis. *Geofluids*, 1(1):2–10, 2002. 14
- [33] B.H. Stuart. *Infrared Spectroscopy: Fundamentals and Applications*. Analytical Techniques in the Sciences (AnTs) *. Wiley, 2004. ISBN 9780470854280. URL <http://books.google.co.uk/books?id=VhYWH0I3fb8C>. 14, 18
- [34] Li Zhou, Chao Gao, Dandan Zhu, Weijian Xu, Fanqing Frank Chen, Amit Palkar, Luis Echegoyen, and Eric Siu-Wai Kong. Facile functionalization of multilayer fullerenes (carbon nano-onions) by nitrene chemistry and "grafting from" strategy. *Chemistry (Weinheim an der Bergstrasse, Germany)*, 15(6):1389–96, January 2009. ISSN 1521-3765. doi: 10.1002/chem.200801642. URL <http://www.ncbi.nlm.nih.gov/pubmed/19115308>. 16
- [35] Gerhard Wenz. Cyclodextrins as Building Blocks for Supramolecular Structures and Functional Units. *Angewandte Chemie International Edition in English*, 33(8):803–822, May 1994. ISSN 0570-0833. doi: 10.1002/anie.199408031. URL <http://doi.wiley.com/10.1002/anie.199408031>. 16
- [36] Shashadhar Samal, Bum-Jin Choi, and Kurt E. Geckeler. The first water-soluble main-chain polyfullerene. *Chemical Communications*, 60(15):1373–

REFERENCES

- 1374, 2000. ISSN 13597345. doi: 10.1039/b003881o. URL <http://xlink.rsc.org/?DOI=b003881o>. 16, 24
- [37] Jae Young Yang, Byung Te Jung, and Dong Hack Suh. A simple attempt to change the solubility of polyimide by physical inclusion with β -cyclodextrin and its derivatives. *Polymer*, 42(20):8349–8354, September 2001. ISSN 00323861. doi: 10.1016/S0032-3861(01)00337-8. URL <http://linkinghub.elsevier.com/retrieve/pii/S0032386101003378>. 17, 18, 21
- [38] World Health Organization., International Labour Organisation., United Nations Environment Programme., and International Program on Chemical Safety. *Dimethylformamide (DMF) health and safety guide*. World Health Organization, Geneva :, 1990. ISBN 9241510439. 24
- [39] Francesco Giacalone, Francesca DAnna, Rosalia Giacalone, Michelangelo Gruttadauria, Serena Riela, and Renato Noto. Cyclodextrin-[60]fullerene conjugates: synthesis, characterization, and electrochemical behavior. *Tetrahedron Letters*, 47(46):8105–8108, November 2006. ISSN 00404039. doi: 10.1016/j.tetlet.2006.09.052. URL <http://linkinghub.elsevier.com/retrieve/pii/S0040403906018508>. 24
- [40] Jiaxing Huang and Richard B Kaner. A general chemical route to polyaniline nanofibers. *Journal of the American Chemical Society*, 126(3):851–5, January 2004. ISSN 0002-7863. doi: 10.1021/ja0371754. URL <http://www.ncbi.nlm.nih.gov/pubmed/14733560>. 28, 30, 47
- [41] G.G. Wallace, G.M. Spinks, and L.A.P. Kane-Maguire. *Conductive Electroactive Polymers: Intelligent Polymer Systems*. CRC PressINC, 2009. ISBN 9781420067095. URL <http://books.google.co.uk/books?id=nEXElsTg23YC>. 28, 29
- [42] Jin-Chih Chiang and Alan G MacDiarmid. Polyaniline: Protonic acid doping of the emeraldine form to the metallic regime. *Synthetic Metals*, 13(13):193 – 205, 1986. ISSN 0379-6779. doi: 10.1016/0379-6779(86)90070-6. URL <http://www.sciencedirect.com/science/article/pii/>

REFERENCES

- [0379677986900706](#). Proceedings of the Workshop "Synthetic Metals III".
28
- [43] W S Huang and A G Macdiarmid. Polaron lattice in highly conducting polyaniline: Theoretical and optical studies. *Physical review ...*, 59(13), 1987. URL <http://link.aps.org/doi/10.1103/PhysRevLett.59.1464>.
28, 45
- [44] G B Street. Polarons, Bipolarons, and Solitons in Conducting Polymers. 1305(4):309–315, 1985. 28
- [45] Mark A Ratner, Bill Davis, Mathieu Kemp, and Vladimiro Mujica. *Molecular Wires : Charge Transport, Mechanisms, and Control*. 2006. 28
- [46] L.A. Samuelson, A. Anagnostopoulos, K.S. Alva, J. Kumar, and S.K. Tripathy. Biologically derived conducting and water soluble polyaniline. *Macromolecules*, 31(13):4376–4378, 1998. 28
- [47] Jing Luo, Sisi Jiang, Yong Wu, Meiling Chen, and Xiaoya Liu. Synthesis of stable aqueous dispersion of graphene/polyaniline composite mediated by polystyrene sulfonic acid. *Journal of Polymer Science Part A: Polymer Chemistry*, 50(23):4888–4894, December 2012. ISSN 0887624X. doi: 10.1002/pola.26316. URL <http://doi.wiley.com/10.1002/pola.26316>. 28
- [48] Ying Dan Liu, Fei Fei Fang, and Hyoungh Jin Choi*. Silica nanoparticle decorated polyaniline nanofiber and its electrorheological response. *Soft Matter*, 7(6):2782, 2011. ISSN 1744-683X. doi: 10.1039/c0sm01279c. URL <http://xlink.rsc.org/?DOI=c0sm01279c>. 29
- [49] T. He, J. Li, L. Wang, J. Zhu, and W. Jiang. Preparation and consolidation of alumina/graphene composite powders. *Materials transactions*, 50(04): 749–751, 2009. 29, 39
- [50] Yongchao Si and ET Samulski. Synthesis of water soluble graphene. *Nano letters*, 2008. URL <http://pubs.acs.org/doi/abs/10.1021/nl080604h>.
29

REFERENCES

- [51] KS Novoselov, AK Geim, SV Morozov, D. Jiang, Y. Zhang, SV Dubonos, IV Grigorieva, and AA Firsov. Electric field effect in atomically thin carbon films. *Science*, 306(5696):666–669, 2004. 29
- [52] K.I. Bolotin, K.J. Sikes, Z. Jiang, M. Klima, G. Fudenberg, J. Hone, P. Kim, and H.L. Stormer. Ultrahigh electron mobility in suspended graphene. *Solid State Communications*, 146(9-10):351–355, June 2008. ISSN 00381098. doi: 10.1016/j.ssc.2008.02.024. URL <http://linkinghub.elsevier.com/retrieve/pii/S0038109808001178>. 29
- [53] Chelsea R. Martinez and Brent L. Iverson. Rethinking the term pi-stacking. *Chemical Science*, 3(7):2191, 2012. ISSN 2041-6520. doi: 10.1039/c2sc20045g. URL <http://xlink.rsc.org/?DOI=c2sc20045g>. 29
- [54] Cristina Vall, Pablo Jim, Edgar Mu, Ana M Benito, and Wolfgang K Maser. Simultaneous Reduction of Graphene Oxide and Polyaniline : Doping-Assisted Formation of a Solid-State Charge-Transfer Complex. *The Journal of Physical Chemistry C*, 115:10468–10474, 2011. 29
- [55] Hualan Wang, Qingli Hao, Xujie Yang, Lude Lu, and Xin Wang. Graphene oxide doped polyaniline for supercapacitors. *Electrochemistry Communications*, 11(6):1158–1161, June 2009. ISSN 13882481. doi: 10.1016/j.elecom.2009.03.036. URL <http://linkinghub.elsevier.com/retrieve/pii/S1388248109001568>. 29
- [56] Lu Mao, Kai Zhang, Hardy Sze On Chan, and Jishan Wu. Surfactant-stabilized graphene/polyaniline nanofiber composites for high performance supercapacitor electrode. *Journal of Materials Chemistry*, 22(1):80, 2012. ISSN 0959-9428. doi: 10.1039/c1jm12869h. URL <http://xlink.rsc.org/?DOI=c1jm12869h>. 29
- [57] Kai Zhang, Li Li Zhang, X. S. Zhao, and Jishan Wu. Graphene/Polyaniline Nanofiber Composites as Supercapacitor Electrodes. *Chemistry of Materials*, 22(4):1392–1401, February 2010. ISSN 0897-4756. doi: 10.1021/cm902876u. URL <http://pubs.acs.org/doi/abs/10.1021/cm902876u>. 29, 36, 40

REFERENCES

- [58] Ying Dan Liu, Fei Fei Fang, and Hyoung Jin Choi. Silica nanoparticle decorated conducting polyaniline fibers and their electrorheology. *Materials Letters*, 64(2):154–156, January 2010. ISSN 0167577X. doi: 10.1016/j.matlet.2009.10.031. URL <http://linkinghub.elsevier.com/retrieve/pii/S0167577X09007940>. 30
- [59] WE Acree. Thermodynamic properties of organic compounds: enthalpy of fusion and melting point temperature compilation. *Thermochimica acta*, 189(1):37–56, October 1991. ISSN 00406031. doi: 10.1016/0040-6031(91)87098-H. URL <http://linkinghub.elsevier.com/retrieve/pii/004060319187098H><http://www.sciencedirect.com/science/article/pii/004060319187098H>. 30
- [60] Hualan Wang, Qingli Hao, Xujie Yang, Lude Lu, and Xin Wang. Graphene oxide doped polyaniline for supercapacitors. *Electrochemistry Communications*, 11(6):1158–1161, June 2009. ISSN 13882481. doi: 10.1016/j.elecom.2009.03.036. URL <http://linkinghub.elsevier.com/retrieve/pii/S1388248109001568>. 31
- [61] Daniela C Marcano, Dmitry V Kosynkin, Jacob M Berlin, Alexander Sinitiskii, Zhengzong Sun, Alexander Slesarev, Lawrence B Alemany, Wei Lu, and James M Tour. Improved synthesis of graphene oxide. *ACS nano*, 4(8):4806–14, August 2010. ISSN 1936-086X. doi: 10.1021/nn1006368. URL <http://www.ncbi.nlm.nih.gov/pubmed/21286599>. 31, 45
- [62] Wen Ling Zhang, Bong Jun Park, and Hyoung Jin Choi. Colloidal graphene oxide/polyaniline nanocomposite and its electrorheology. *Chemical communications (Cambridge, England)*, 46(30):5596–8, August 2010. ISSN 1364-548X. doi: 10.1039/c0cc00557f. URL <http://www.ncbi.nlm.nih.gov/pubmed/20577695>. 32
- [63] Chengmeng Chen, Quan-Hong Yang, Yonggang Yang, Wei Lv, Yuefang Wen, Peng-Xiang Hou, Maozhang Wang, and Hui-Ming Cheng. Self-Assembled Free-Standing Graphite Oxide Membrane. *Advanced Materials*, 21(29):3007–3011, August 2009. ISSN 09359648. doi: 10.1002/adma.200803726. URL <http://doi.wiley.com/10.1002/adma.200803726>. 33, 45

REFERENCES

- [64] Jéssica Alves Marins and Bluma Guenther Soares. A facile and inexpensive method for the preparation of conducting polyanilineclay composite nanofibers. *Synthetic Metals*, 162(23):2087–2094, December 2012. ISSN 03796779. doi: 10.1016/j.synthmet.2012.10.015. URL <http://linkinghub.elsevier.com/retrieve/pii/S037967791200361X>. 45
- [65] JJ van Hapert. *Hopping Conduction and Chemical Structure : a study on Silicon Suboxides*. Phd thesis, Utrecht University, 2002. URL <http://igitur-archive.library.uu.nl/dissertations/2002-0806-101243/UUindex.html>. 45
- [66] P Stallinga. Electronic transport in organic materials: comparison of band theory with percolation/(variable range) hopping theory. *Advanced materials (Deerfield Beach, Fla.)*, 23(30):3356–62, August 2011. ISSN 1521-4095. doi: 10.1002/adma.201101129. URL <http://www.ncbi.nlm.nih.gov/pubmed/21671450>. 45
- [67] M Campos and B Bello Jr. Mechanism of conduction in doped polyaniline. *Journal of Physics D: Applied Physics*, 1531, 1999. URL <http://iopscience.iop.org/0022-3727/30/10/021>. 46
- [68] Eduardo V. Castro, H. Ochoa, M. I. Katsnelson, R. V. Gorbachev, D. C. Elias, K. S. Novoselov, a. K. Geim, and F. Guinea. Limits on Charge Carrier Mobility in Suspended Graphene due to Flexural Phonons. *Physical Review Letters*, 105(26):266601, December 2010. ISSN 0031-9007. doi: 10.1103/PhysRevLett.105.266601. URL <http://link.aps.org/doi/10.1103/PhysRevLett.105.266601>. 46
- [69] H. Ochoa, Eduardo V. Castro, M. I. Katsnelson, and F. Guinea. Temperature-dependent resistivity in bilayer graphene due to flexural phonons. *Physical Review B*, 83(23):235416, June 2011. ISSN 1098-0121. doi: 10.1103/PhysRevB.83.235416. URL <http://link.aps.org/doi/10.1103/PhysRevB.83.235416>. 46
- [70] H Ochoa and EV Castro. Scattering by flexural phonons in suspended graphene under back gate induced strain. *Physica E: Low- ...*,

REFERENCES

- (3), 2011. URL <http://www.sciencedirect.com/science/article/pii/S1386947711000919>. 46
- [71] J Schiefele, Fernando Sols, and F Guinea. Temperature dependence of the conductivity of graphene on boron nitride. *Physical Review B*, pages 1–6, 2012. URL <http://prb.aps.org/abstract/PRB/v85/i19/e195420>. 46
- [72] SD Sarma, S Adam, EH Hwang, and Enrico Rossi. Electronic transport in two dimensional graphene. *arXiv preprint arXiv:1003.4731*, pages 1–69, 2010. URL <http://arxiv.org/abs/1003.4731>. 46
- [73] Shuiping Zhou, Hongming Zhang, Qiang Zhao, Xianhong Wang, Ji Li, and Fosong Wang. Graphene-wrapped polyaniline nanofibers as electrode materials for organic supercapacitors. *Carbon*, 52:440–450, February 2013. ISSN 00086223. doi: 10.1016/j.carbon.2012.09.055. URL <http://linkinghub.elsevier.com/retrieve/pii/S0008622312008032>. 50
- [74] Innam Lee, Seong Yong Park, Moon J Kim, and Minhee Yun. Materialization of single multicomposite nanowire: entrapment of ZnO nanoparticles in polyaniline nanowire. *Nanoscale research letters*, 6(1): 393, January 2011. ISSN 1556-276X. doi: 10.1186/1556-276X-6-393. URL <http://www.pubmedcentral.nih.gov/articlerender.fcgi?artid=3211487&tool=pmcentrez&rendertype=abstract>. 50